2018

# DESIGN OF A TENDON DRIVEN SOFT CONTINUUM ROBOTIC ARM USING PROPRIOCEPTIVE SENSORS

Richard Sperling
*University of Rhode Island*, r-sperling@my.uri.edu

# DESIGN OF A TENDON DRIVEN SOFT CONTINUUM ROBOTIC ARM USING PROPRIOCEPTIVE SENSORS

BY

RICHARD SPERLING

A THESIS SUBMITTED IN PARTIAL FULFILLMENT OF THE

REQUIREMENTS FOR THE DEGREE OF

MASTER OF SCIENCE

IN

MECHANICAL ENGINEERING

UNIVERSITY OF RHODE ISLAND

2018

MASTER OF SCIENCE THESIS

OF

RICHARD SPERLING

APPROVED:

Thesis Committee:

Major Professor

Hongyan Yuan

Chengzhi Yuan

Brennan Phillips

Nasser H. Zawia
DEAN OF THE GRADUATE SCHOOL

UNIVERSITY OF RHODE ISLAND

2018

**Abstract**

In this thesis the use of proprioceptive sensors in elephant trunk inspired soft continuum robots was explored. After presenting the basics for this project, a review of existing soft continuum robots is given. The sensors used are off-the-shelf stretch senors. Those sensors are carbon black impregnated rubber cords. The design and the fabrication of the robot are described. Using material characteristics a calibration process was developed to improve the sensor's consistency. The robot is then tested in open-loop as well as a closed-loop experiment. Results of those experiments are presented and discussed.

**Acknowledgment**

I would first like to thank my thesis advisor Dr. Hongyan Yuan of the Department of Mechanical Engineering at the University of Rhode Island. The door to Prof. Yuan office was always open whenever I ran into a trouble spot or had a question about my research or writing. He consistently allowed this project to be my own work, but steered me in the right direction whenever he thought I needed it.

I would also like to acknowledge Bahador Marzban and Reed Nelson of the Department of Mechanical Engineering at the University of Rhode Island, who supported me in conducting the experiments and offered me their opinion on the current state of the project.

## Contents

**List of Figures**

**List of Tables**

## List of Algorithms

**Nomenclature**

| | |
|---|---|
| $\alpha_i$ | Angle of sensors |
| $\delta$ | Distance of tendons/sensors from the center of the robot |
| $\ell$ | Length along thread in the center |
| $\kappa$ | Bending curvature |
| $\mathbf{q}$ | Actuator space |
| $\mathbf{s}$ | Sensor space |
| $\mathbf{x}$ | Task space |
| $\phi$ | Angle to bending plane |
| $\theta$ | Bending angle |
| $\varphi_i$ | Angle of tendons |
| $\vec{p}$ | End-effector position in bending plane |
| $I$ | Electric current |
| $l_i$ | Tendon lengths |
| $N_{actuators}$ | Number of actuators |
| $r$ | Bending radius |

| | |
|---|---|
| $R_C$ | Electric stretch sensor resistance |
| $R_{PD}$ | Pull-down resistance |
| $s_i$ | Sensor lengths |
| $T$ | Transformation matrix |
| $T_\phi$ | Transformation matrix for bending direction |
| $T_{r,\theta}$ | Transformation matrix in bending plane |
| $V_{in}$ | Input voltage |
| $V_{out}$ | Output/measured voltage |
| $V_{R_C}$ | Voltage drop over $R_C$ |
| $x$ | x-Coordinate of end-effector |
| $x_{ci}$ | x-Coordinate of tendons on xy-plane |
| $x_{si}$ | x-Coordinate of sensors on xy-plane |
| $y$ | y-Coordinate of end-effector |
| $y_{ci}$ | y-Coordinate of tendons on xy-plane |
| $y_{si}$ | y-Coordinate of sensors on xy-plane |
| $z$ | z-Coordinate of end-effector |

## 1 Introduction

To mimic the locomotion and manipulation mechanisms of soft biological organisms, soft robotics have been attracting intensive research interests [109] recently. Soft robots are made primarily of elastomeric materials which undergo large and continuous deformation when subject to actuator (internal) and environmental (external) forces. As a result, soft robots can adapt their shapes to variable, geometrically complex environments [120] and are safe to operate when interacting with humans, animals, or manipulating human tissues/organs [108, 101]. The versatility and adaptability of soft robots make them better suited for open-ended tasks such as navigating in uncertain environments. Applications of soft robots as manipulators include a soft gripper for pick-and-place articulation [55], a soft contractable sleeve as heart assistive device [108], a soft arm for deep-sea exploration [100], a soft actuated system for gait rehabilitation [101]. Autonomous mobile soft robots have been designed to explore the modes of locomotion, such as a tissue-engineered soft robotic stingray with light sensing [94], a resilient walking soft robot in hazardous conditions [120], and a soft robotic fish capable of escape maneuvers [82].While significant advances have been made in the field of soft robotics in recent years, obstacles still exist in fabrication, sensing, modeling and control of soft robots which have prevented full realization of the promising applications of soft robots.

While the compliance of soft robots is an integral part of their functions, it poses a challenge in the sensing of robotic configurations. Many traditional sensors for rigid

robots, such as motor encoders, do not work well for soft robots, especially when the soft robots physically interact with environments. This is because soft robots can undergo large continuum deformation. The kinematic relations that describe the mappings between actuation space, configuration space, and task space of soft robots not only depend on robot geometry, but also material stress-strain relationship and environmental constraints. In the general cases, nonlinear finite-strain elasticity problems need to be solved to obtain the kinematic relations [88, 35], which are computational intensive when solved numerically using the finite element method.

Both external and internal sensors have been explored to acquire the configuration of soft robots. External position tracking systems, such as electromagnetic tracking [49] and optically-based 3D motion capture [45], has been used to obtain shape sensing for feedback control. External sensing systems work well for situations where modestly-sized robots perform tasks in a predefined area which can be covered by the external tracking system. For long distance tasks or large scale robotic designs, such as autonomous mobile robots or extendable robotic arms, a means of internal sensing is preferred. The primary deformation mode of soft robotic arms is bending; therefore, to accurately predict the end-state configuration, it is required to know the curvature along the soft-robotic arm. Several proprioceptive sensors that are able to achieve this have been developed and/or implemented previously. Such sensors include: a Hall Effect sensor [92]; a piezoelectric deflection sensor [113]; a soft-strain sensor which utilizes conductive fabric [33]; fiber-optic sensors [111]. Such sensors, in principle, can measure the local curvature along the

robotic arm. A simpler approach is to assume the curvature along the length of each segment of a modular arm is constant; therefore, measuring the length along different paths in the longitudinal direction of the arm segment allows one to compute the curvature based on the geometric relations. Previous work following this approach includes a length sensor based on inductance change of conductive braids [48], soft-strain sensors which utilize either liquid or carbon nanotube conductors [53], and a commercially available bilayer thin film sensor [50].

Various actuation strategies have been used in soft robotics for locomotion and articulation; these include flexible fluidic actuators [110, 88], tendon-drives [104], shape memory alloys [127], electro-active polymers [91], etc. Among them, the tendon-driven approach, where DC motors pull tendons inside the robotic arm to generate curvature, has several advantages. First, the use of tendon-drive actuation has been extensively proven by in traditional hard continuum robotic arms. The mechanics models developed previously for a tendon-driven continuum arm can be used, modified, and extended to the soft tendon-driven robotic arms. Secondly, because of the softness and light-weight nature of soft robotic arms, small batteries and miniature motors will suffice for actuation.

In this work, we explore the curvature sensing using conductive soft filaments for the feedback control of a tendon-driven soft robotic arm. Ideally, a low-cost proprioceptive sensor made of soft materials is preferred such that it does not restrict the deformation of soft robots in any directions.

## 2 Basics

In this section the basic knowledge of for this project will be presented. This includes:

- the mathematical description of robots (subsection 2.1)
- the usage of MCU (Micro Controller Units) as interface between hardware and software

## 2 Kinematics

In robotics a common way to find a end-effector position for a robot is by using a homogeneous transformation. With a known homogeneous transformation matrix $T$ and known base coordinates $x_b$, $y_b$, and $z_b$, the end-effector coordinates $x_e$, $y_e$, and $z_e$ can be derived using Equation 2.1. $R$ describes the rotation of the base and $\vec{t}$ the translation of the base.

$$\begin{bmatrix} x_e \\ y_e \\ z_e \\ 1 \end{bmatrix} = \underbrace{\begin{bmatrix} & R & & \vec{t} \\ 0 & 0 & 0 & 1 \end{bmatrix}}_{T} \begin{bmatrix} x_b \\ y_b \\ z_b \\ 1 \end{bmatrix} \tag{2.1}$$

The transformation matrix $T$ dependent on the actuator states. For example: A tendon driven robot this with 3 tendons would have a transformation matrix that is dependent on the 3 tendon lengths $T(l_1, l_2, l_3)$. Mapping the actuator states to the end-effector position is known as forward kinematics. Mapping the end-effector coordinates to the

actuator states is called inverse kinematics and requires solving the system of equations (Equation 2.1).

## 2 Micro Controller Unit

MCUs (**M**icro **C**ontroller **U**nit) are small computer in an integrated circuit. On those MCUs small code (due to limited memory) can be run and specific Voltages on physical pins can be output or measured. A few examples of MCUs are shown in Figure 2.1.

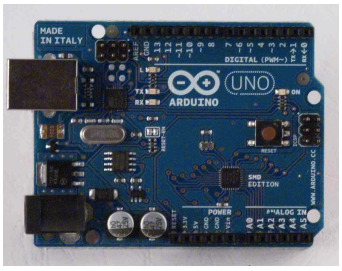


(a) Arduino Uno SMD [7]

(b) Arduino Pro Mini [6]

(c) ESP-12E [93]

Figure 2.1: Different MCUs

The main difference between the Arduino Uno (see Figure 2.1a) and the Arduino Pro Mini (see Figure 2.1b) is the size and the number of pins. Also the Arduino Pro Mini doesn't have a USB to TTL serial converter like the Arduino Uno. The ESP-12E uses a different processor than the Arduino chips and requires only a 3.3 V power supply. However it can therefor output a maximum of 3.3 V. The ESP-12E MCU also has a ESP8266 WiFi Module.

MCUs posses 3 different types of pins:

- digital IO pins
- analog input pins
- PWM output pins (can also be used as digital IO pins)

Digital IO pins have to be set to either input or output mode. In input mode the MCU read a high voltage if the potential at the pin is above a certain threshold () and reads a low voltage otherwise. In output mode the MCU can set the potential at the pin to a high voltage (5 V) or a low voltage (0 V).

To program those MCUs the Arduino IDE can be used. This software allows the user to program using a programing language that is similar to c++. Instead of a main function the Arduino language uses a setup function and a loop function. The setup function is executed once, when the MCU is started (or the reset button is pressed). After that the loop function is executed repeatedly.

## 2 Measuring Resistance using an MCU

To measure a unknown resistance using an Arduino board the circuit is setup as shown in Figure 2.2a. A schematic of this circuit is shown in Figure 2.2b. Here one of the analog input pins is used to measure the voltage drop over the pull-down resistor. The analog inputs in the range of 0 V

In terms of this project the unknown resistor will be replaced with the sensors (conductive rubber cords). Here $V_{in}$, $R$ (pull-down resistor) and $V_{out}$ are known. The pull-down

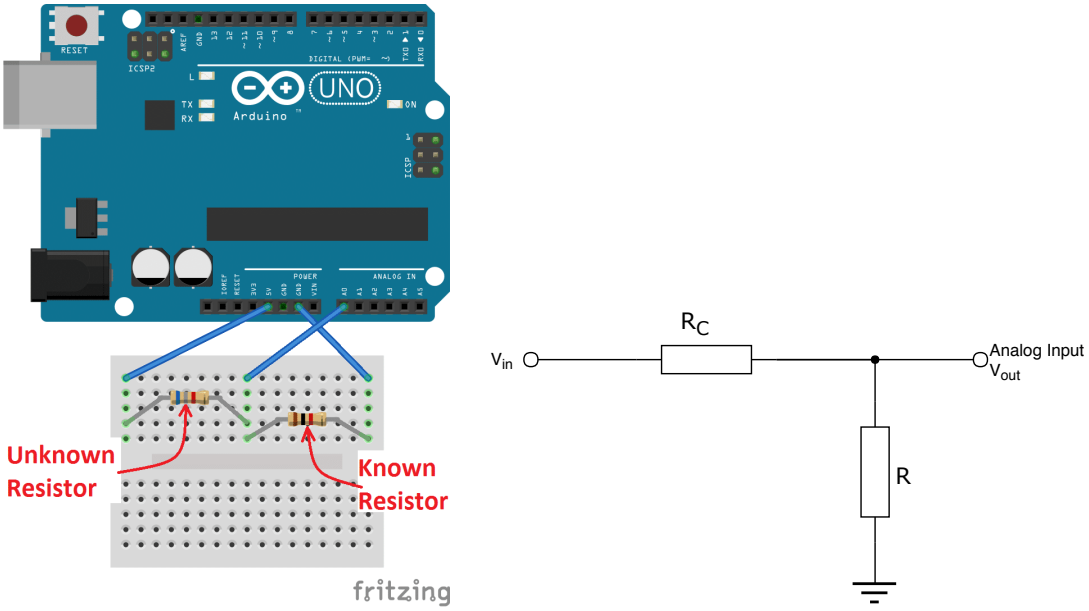


(a) Ohm meter circuit [12]

(b) Ohm meter schematic

Figure 2.2: Ohm meter using a MCU

resistor is required to prevent current from flowing into the analog input. The current flowing through both resistors must be equal:

$$I = \frac{V_{out}}{R} = \frac{V_{R_C}}{R_C} \tag{2.2}$$

According to Kirchhoff's second law Equation 2.3 holds.

$$V_{in} = V_{R_C} + V_{out} \tag{2.3}$$

From those equations $R_C$ can be derived:

$$R_C = \left( \frac{V_{in}}{V_{out}} - 1 \right) R \tag{2.4}$$

Because a MCU doesn't read analog voltage values, but instead converts those to digital values, we have to deal with errors during the readings. Section 2.2.1 shows the error of the measurement in dependence of the actual resistance of the unknown resistance. The error has its minimum for a resistance value similar to the pull-down resistor.

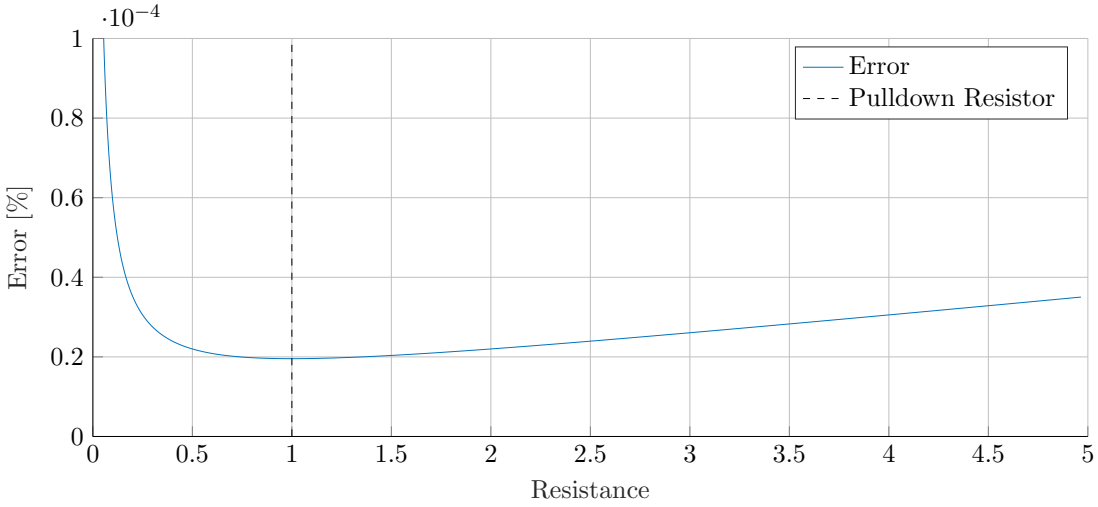


Figure 2.3: Error of measuring Resistance

## 2 Interrupt Functions

To trigger functions in through a signal applied at the input pins Arduino Boards offer interrupt functions. Whenever a event (rising voltage, falling voltage) occurs at a pin

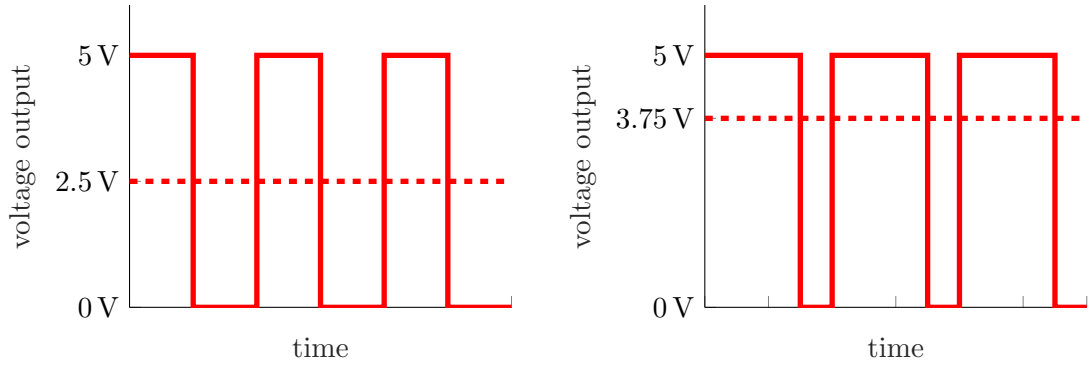


(a) 50 % Duty cycle (b) 75 % Duty cycle

Figure 2.4: PWM examples

with an interrupt function attached to it, the execution of the code is paused and the interrupt function is executed. After that the program continues where it was paused. This feature can be used to detect voltage peaks. In this project interrupt functions are used in combination with motor encoders.

## 2 Pulse Width Modulation

Pulse width modulation is a method to create a analog voltage by switching between 2 different voltage potentials. By changing the width of a pulse (high voltage level) without changing the width for a whole cycle a different average voltage can be achieved. Even though this technically is not a analog voltage output, in many electronic circuits it can be treated as one, because PWM usually uses a very high frequency. Figure 2.4a shows a example for a 50 % duty cycle with a 0 V and a 5 V potential. The voltage output is 2.5 V. Figure 2.4b shows a 75 % duty cycle with a 3.75 V output.

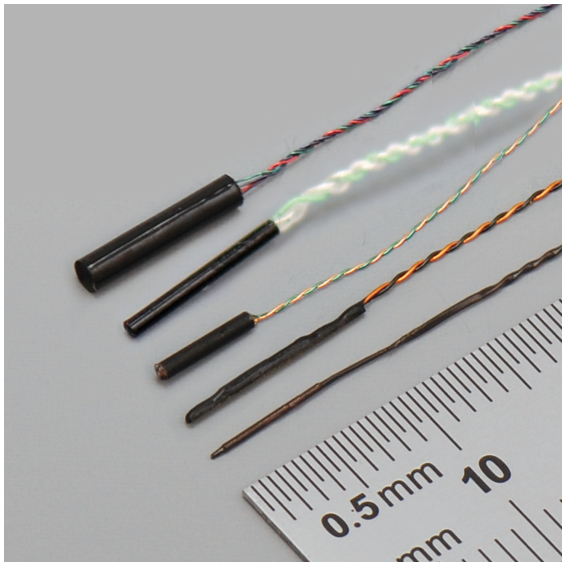


Figure 2.5: EM sensors [89]

### 2 Electromagnetic Tracking Sensor

Electromagnetic tracking sensor are sensors that can be used to track a position and orientation accurately. The system consists of a field generator that creates a oscillating electromagnetic field. Sensors such as those shown in Figure 2.5 consist of small solenoids. Due to the electromagnetic field a current is induced in those solenoids. Depending on the location and orientation of the sensors different currents are induced in the solenoids. With this data the position and orientation of the sensors relative to the field generator can be tracked.

The accuracy of those sensors decreases when disruptive factors are near. Because the sensors rely on the electromagnetic field, any kind of ferromagnetic material or electric current nearby introduces a error.


Figure 2.6: EM field generator [89]

## 3 State of the Art

Most soft robots can also be classified as continuum robots. Therefor the following sections describe those continuum robots. After that a introduction to soft robots is given.

## 3 Continuum Robots

Continuum robots are robots that manly move by deforming parts. In this section the focus wil be put on elephant trunk or snake shaped robots. Those continuum robots can be compared using different criteria [115, 59, 107, 128]:

- continuous or discrete
- extensibility
- number of sections
- actuators per section
- DOF per section
- actuator spacing
- actuation

Table 3.1 shows robots used in literature with their respective criteria.

| Reference | *Continuous / discrete* | *Extensible* | *Number of sections* | *Actuators per section* | *DOF per section* | *Actuator spacing* | *Actuation* |
|---|---|---|---|---|---|---|---|
| [63, 64] | C | ✓ | 3 | 2 | 2 | 180° | P |
| [65] | C | (✓) | 1 | 1 | 1 | - | T |
| [85] | C | ✓ | 3 | 3 | 3 | 120° | P |
| [44] | C | ✓ | 1 | 3 | 3 | 120° | P |
| [87] | C | ✗ | 1 | 1 | 1 | - | P |
| [20] | C | ✗ | 1 | 5 | 2 | non uniform | T |
| [10] | C | ✓ | 1 | 3 | 3 | 120° | T |
| [70, 69] | C | ✓ | 1 | 4 | 4 | 120 ° | T |
| [88] | C | (✓) | 1 | 1 | 1 | - | P |
| [51] | C | ✗ | 1 | 2 | 2 | 180° | P |
| [49] | C | ✓ | 2 | 3 | 3 | 120° | T |
| [102] | C | ✗ | 1 | 1 | 1 | - | T/P |
| [78] | C | ✓ | 1 | 6 | 6 | 60° | T/P |
| [75] | C | ✗ | 2 | 1 | 1 | - | T |
| [54] | C | ✓ | 1 | 2 | 2 | 180° | T |
| [103, 104] | C | ✓ | 1 | 4 | 3 | 90° | T |
| [80, 81, 83, 84] | C | ✓ | 6 | 2 | 2 | 180° | P |
| [26] | C | ✗ | 1 | 1 | 1 | - | T |
| [22] | C | (✓) | 1 | 1 | 1 | - | T |
| [97] | C | ✓ | 1 | 4 | 3 | 90° | T |
| [116] | C | ✓ | 1 | 2 | 2 | 180° | P |
| [90] | C | ✓ | 1 | 3 | 3 | 120° | P |
| [86] | C | ✓ | 2 | 3 | 3 | 120° | P |

Table 3.1: Properties of robots used in literature (extension to table in [128])

### 3 Continuous and Discrete Robots

A Continuous robot is one that moves by deforming parts. A discrete robot is one that moves by having parts that purely rotate or translate. However many discrete robots have a very high number of small joints. Due to the high number of joints a approximation as continuum robot can be made. If those joints can be actuated individually those robots become highly redundant as every joint adds additional DOF. [128]

### 3 Extensibility

The extensibility of a robot describes whether compression and lengthening of the body is taken into account or whether the robot purely bends. For a inextensible robot the number of linear independent DOF of a section is capped to 2. A extensible robot on the other hand can have up to 3 linear independent DOF. [128]

### 3 Number of Sections

For a robot that consists of more than one section, more DOF are added. Those additional DOF however are not necessarily linear independent and therefor can add redundancy to the whole robot. Despite having multiple sections most robots are capped in the number of sections. This is due to the fact that the actuation of one section still takes place at the base of the robot. In this case tendons or tubes for the actuation of the later sections pass through the first sections. [128]

### 3 Actuators per Section

The number of actuators per section is strongly related to number of DOF. A robot with only 2 actuators can only have 2 linear independent DOF. Some robot design contain 4 actuators in one section. By having more than 3 actuators a robot can achieve a bidirectional behavior. Many other robots achieve the bidirectionality by having springs that pull the robot in the other direction or have bidirectional actuators. [128]

### 3 Degrees of Freedom per section

The DOF of a robot represents how complex the movement can be. While 6 DOF would be enough to reach any point in a 3 dimensional space from any direction, it is restricted in path it takes to the point. To deal with restrictions from the environment more DOF are added (usually by adding more sections). [128]

### 3 Actuator Spacing

The actuator spacing describes the location of the actuators. Snake like robots usually have their actuators located symmetrically around the center. So the actuator spacing is dependent on the number of actuators ($\varphi_{i+1} - \varphi_i = \frac{2\pi}{N_{actuators}}$). [128]

### 3 Actuation

The actuation in many cases is done using tendons or hydraulic/pneumatic pumps. While it is usually easy for a pump to achieve big bending angles due to high pressure,

| **Hydraulic/Pneumatic** | **Tendons** |
|---|---|
| •high forces | •low forces |
| •high power consumption | •low power consumption (for example by DC-motors) |
| •heavy pump required | •motors can be lightweight |
| •slow actuation | fast actuation |
| •complicated kinematic model requires FEM or approximated mapping function | •simple closed form kinematics |

Table 3.2: Comparison between hydraulic/pneumatic actuation and tendon driven actuation

they bring a few disadvantages with them. Table 3.2 shows a comparison between hydraulic/pneumatic actuation and tendon driven actuation. The fact that a tendon driven robot could possibly carry its own actuation makes such a system suitable for mobile applications. [128]

## 3 Soft Robots

In soft robotics the robots are made out of a soft material such as silicon rubber instead of rigid joints and arms. Usually those robot are classified as continuous robots as their main way of moving is through elastic deformation of the soft material. Examples for inspiration from nature are shown in Figure 3.1. Pneumatic or hydraulic actuation is widely popular for those kinds of robots as the pressure chambers can easily be embedded in the robot's body. [85, 87, 88, 51, 102, 118]

In [82] a fish like robot was developed (see Figure 3.2a), that was capable of maneu-

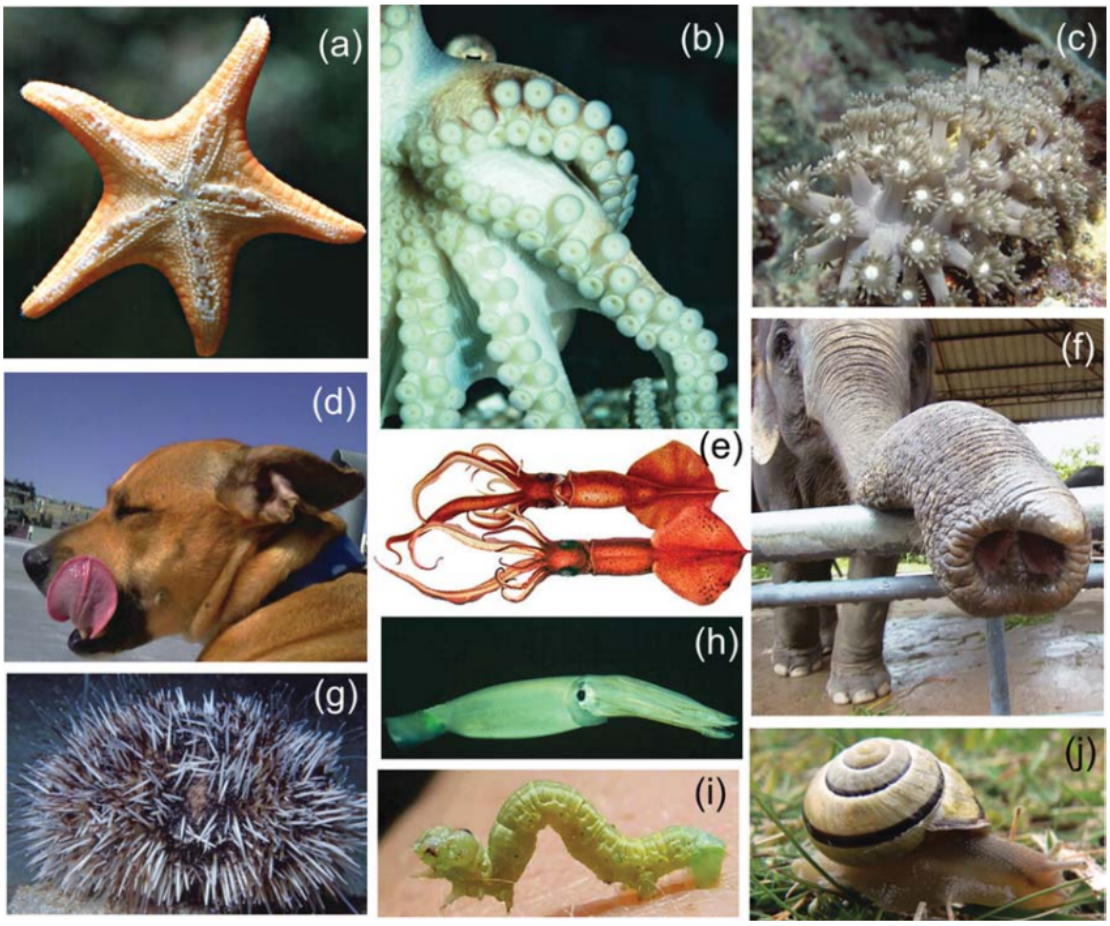


Figure 3.1: Examples of hydroskeletons and muscular hydrostats: (a) tube feet in starfish, (b) octopus arms, (c) colonial anemone, (d) mammalian tongue, (e) squid, (f) elephant trunk, (g) echinoid, (h) Illex illecebrosus, (i) inchworm, and (j) snail feet. [123]

vering through water by actuating its tail. One of the advantages of a application in water is that gravitational effects on the soft material are very low as the density of the silicon rubber is similar to water. In [104, 106] (robots in Figures 3.2b and 3.2e) the developed robot makes use of this property by conducting the experiments in a water tank. This environmental advantage is even stronger in applications in space due to the complete absence of gravity and surrounding medium. [121] Other applications of soft robots are mobile robots for geometrically complex environments (Figure 3.2d) or gripper for sensitive objects (Figure 3.2c).

Many soft robots are inspired by an elephant trunk, an octopus arm or a snake. So a lot of research has been done on the kinematics and control of those kind of robots. To obtain a kinematical model [20, 10] derived equations using the tendon tress. In those cases material properties of the soft deforming body have to be well known. Another approach uses the displacement of tendons. [128] Those models however do not consider outside forces or gravity. Pneumatically/hydraulically actuated robots don't really have this resource. That is why [90] use a mapping based on sample data. To obtain a more accurate model [44, 87, 88, 42] use a Finite-Element-Method based approach. The downside of those FEM simulations is that they are time consuming and therefor not suited for real time control. Many different types of sensors have been used in order to implement a feedback control:

- a Hall Effect sensor [92]

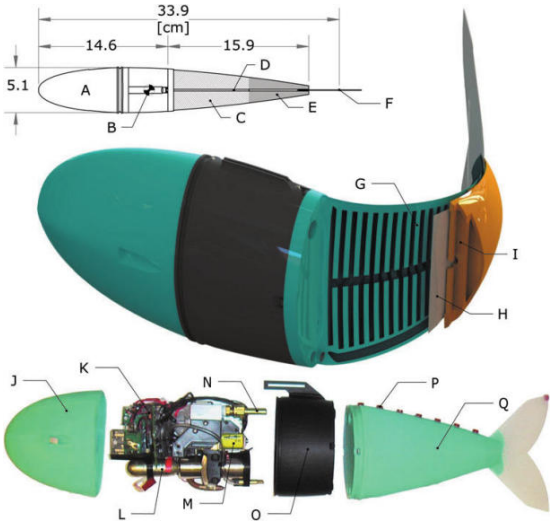


(a) Autonomous soft robotic fish [82]

(b) Octopus arm inspired robot [104]

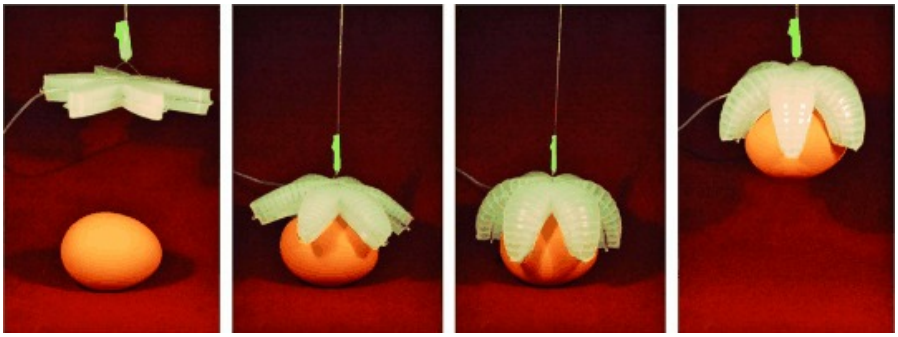

(c) Soft robotic gripper [60]

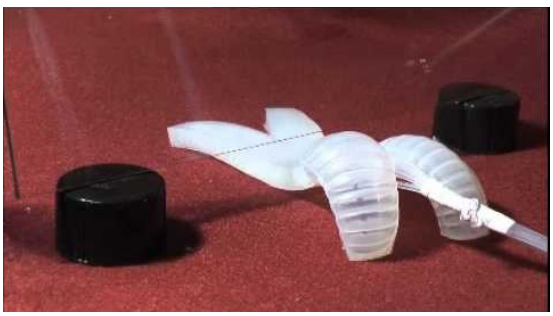

(d) Soft robotic walker [114]

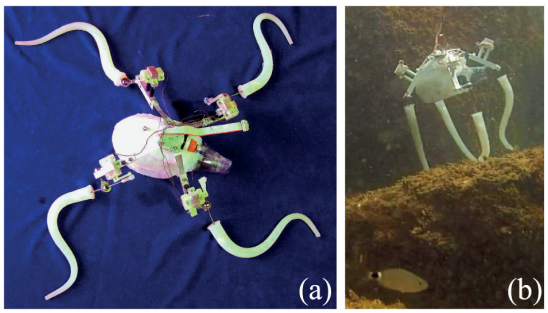


(e) Multi-body aquatic vehicle [106]

Figure 3.2: Different robot designs in literature

- a piezoelectric deflection sensor [113]
- a soft-strain sensor which utilizes conductive fabric [33]
- fiber-optic sensors [111]
- a flex bend sensor [52]

Sensors like the Hall Effect sensor [92], the piezoelectric deflection sensor [113] or the flex bend sensor [52] cause a nonuniform bending behavior for 3D bending which limits their applications. [105, 85, 81, 116, 57, 90, 52, 102, 109, 19, 128, 96]

# 4 Experimental Setup

This section describes the experimental setup used. This includes the design, fabrication and control of the robot as well as the mathematical model.

## 4 Robot Design

The designed robot is a arm shaped soft continuum robot made of silicon rubber. Embedded in the robot are 3 carbon-black impregnated rubber cords [2]. The same sensors have been used in [90]. The robot is driven by 3 DC-motors that pull on 3 tendons. The output torque is increased with a gearbox. To prevent the tendons from cutting through the silicon body plastic tubes are used to cover the tendons and protect the rest of the robot. A schematic of the robot is shown in Figure 4.1 and a cross section in Figure 4.2.

Additionally to the stretch sensors and the Hall-effect sensors, electromagnetic tracking sensors are used. Those sensors track the their location in an changing electromagnetic field. One of those sensors is placed at the tip of the robot and one at the base for reference. Using this system the data of the other sensors is validated. Also those sensors are used for calibration of the stretch sensors.

## 4 Fabrication

The silicon rubber used for the robot is a platinum-catalyzed silicon rubber [117]. Table 4.1 shows the material properties of the compared materials. In this project Ecoflex

Figure 4.1: Schematic of the robot (blue = silicon rubber ; black = stretch sensors ; yellow = cables ; grey = plastic tubes)

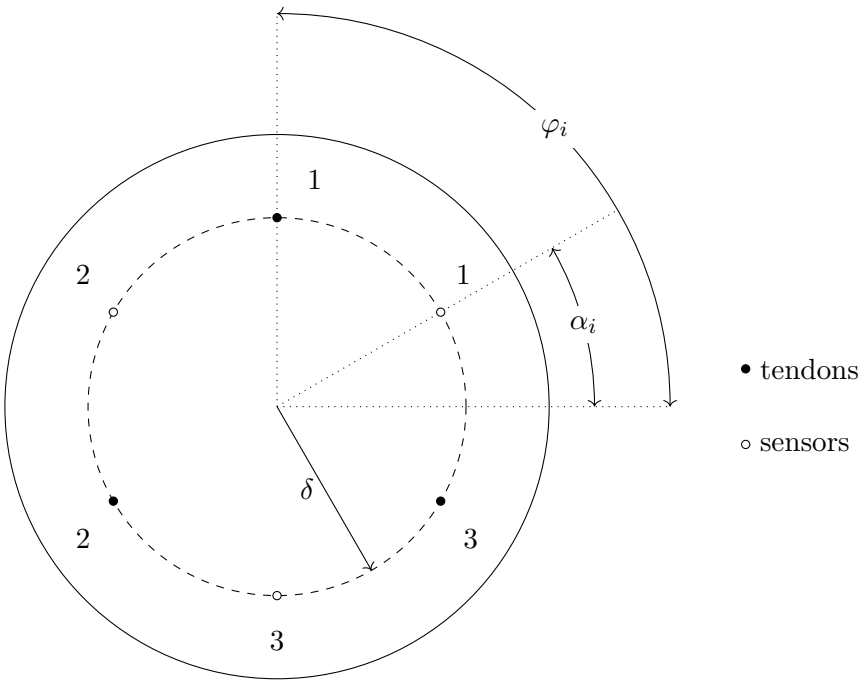


Figure 4.2: robot cross section

| **Property** | **00-10** | **00-20** | **00-30** | **00-35** | **00-50** |
|---|---|---|---|---|---|
| Density | 1070 $\frac{\text{kg}}{\text{m}^3}$ | 1070 $\frac{\text{kg}}{\text{m}^3}$ | 1070 $\frac{\text{kg}}{\text{m}^3}$ | 1070 $\frac{\text{kg}}{\text{m}^3}$ | 1070 $\frac{\text{kg}}{\text{m}^3}$ |
| Cure Time | 4 h | 4 h | 4 h | 5 min | 3 h |
| Tensile Strength | 827 kPa | 1103 kPa | 1379 kPa | 1379 kPa | 2172 kPa |
| 100% Modulus | 55 kPa | 55 kPa | 69 kPa | 69 kPa | 83 kPa |
| max. Elongation | 900 % | 845 % | 900 % | 900 % | 980 % |
| Shrinkage | <0.1 % | <0.1 % | <0.1 % | <0.1 % | <0.1 % |

Table 4.1: Material properties of Ecoflex[117]

00-30 was used as it is soft enough to be bend using small motors. Ecoflex 00-35 was rejected due to the low curing time which would not leave enough time to prepare the mixture and pour it into the mold.

After mixing the two components the mixture is placed in a vacuum chamber to extract air enclosed in it. The mixture is then removed from the chamber and poured into a mold (see Figure 4.3) and cured for at least 4 h. The curing does not take place inside the vacuum chamber as better results are obtained. Steel wires covered with plastic tubes serve as placeholders for the cables and sensors during the curing process. The placeholder for the sensors are removed from the cured arm, while the others remain as protection for the body from the tendons.

The tendons are fixed to the tip of the robot and at the base they are fixed to the DC-motors. When fixing the stretch sensors to the ends of the robot, the arm is first compressed by pulling the tendons. That way the stretch sensors remain under tension during the whole experiments, when the tendons are released. This pretension is necessary to prevent the sensors from rambling when the arm is compressed and thus improve

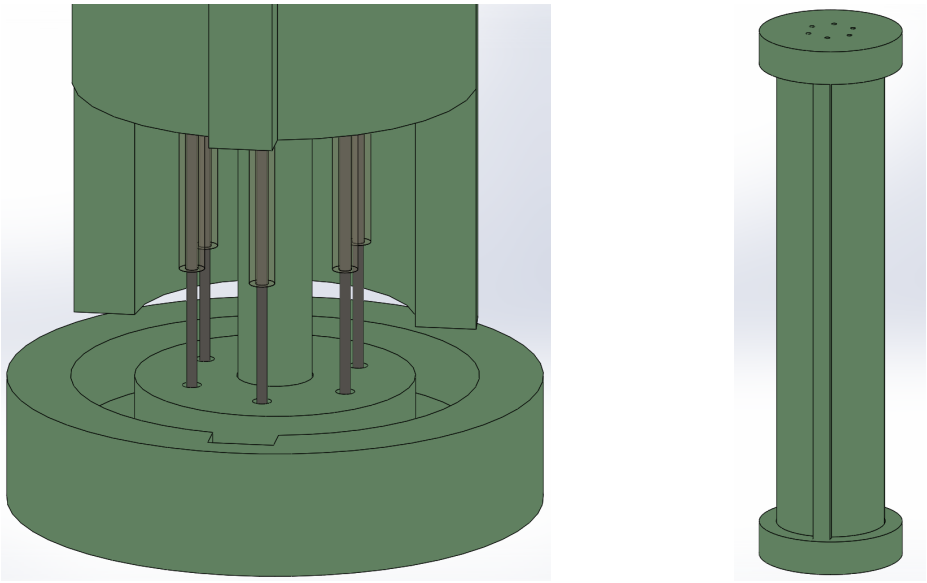

(a) opened mold (b) closed mold

Figure 4.3: Mold used for robot fabrication

the quality of the readings.

During the whole fabrication lubrication is avoided as the sensors are very sensitive to silicon based environments. A more detailed characterization of this behavior is given in Section 5.

## 4 Control

For the control of the robot a Arduino Uno board was used. Figure 4.4 shows the electronic circuit.

The resistance of the stretch sensors are measured by measuring the voltage drop through the pull-down resistors $R_{pd} = 2\,\mathrm{k}\Omega$. For a known input voltage $V_{in} = 5\,\mathrm{V}$ The

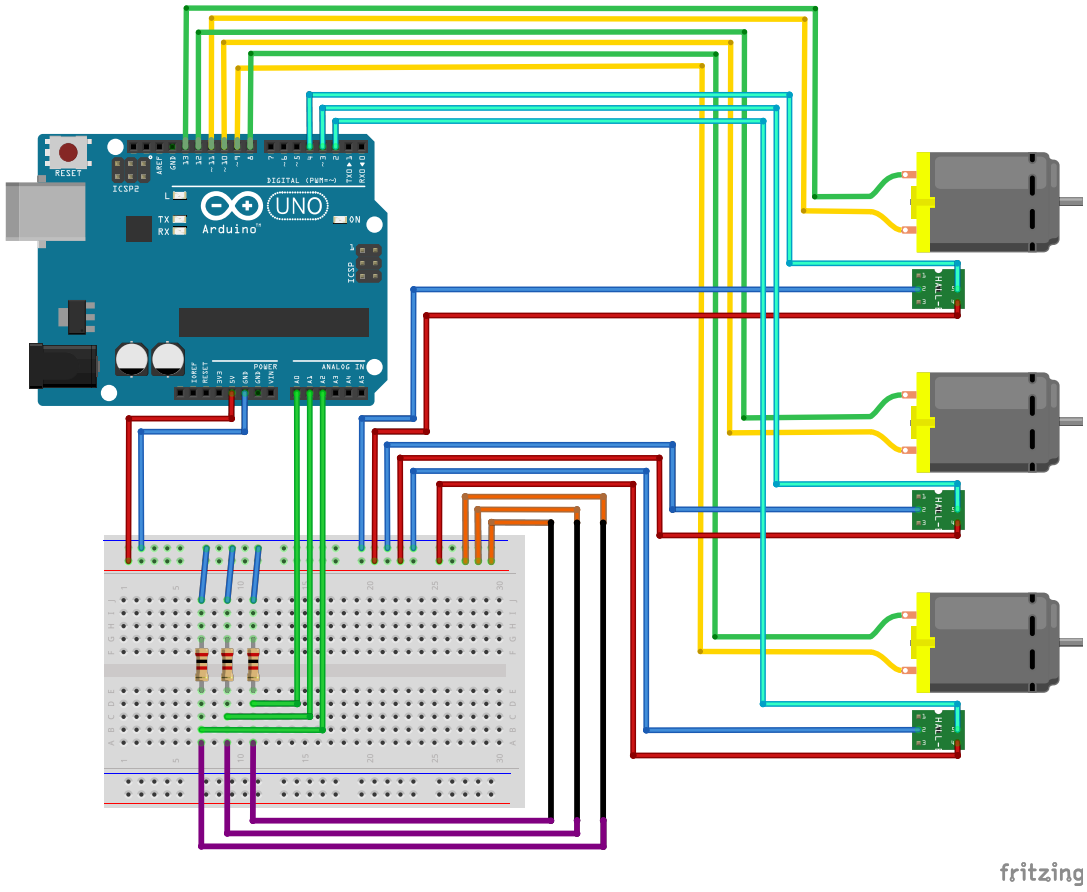


Figure 4.4: Setup of the electronics (black = stretch sensors ; green chips = Hall effect sensors)

resistance can then be calculated using Equation (4.1) (according to Section 2.2.1).

$$R_{sensor} = R_{pd}\left(\frac{V_{in}}{V_{mes}} - 1\right) \tag{4.1}$$

The DC-motors are controlled by using one PWM output of the MCU and one digital output. By setting the voltage outputs of those pins according to Algorithm 1 a bidirectional actuation can be achieved.

**Algorithm 1:** speed output decision logic

```
   Input: speed
1  map speed to voltage V_out;
2  if 0 ≤ V_out then
3  |  set PWM output to V_out;
4  |  set digital output to 0 V;
5  else
6  |  set PWM output to 5 V + V_out;
7  |  set digital output to 5 V;
8  end
```

To use the Hall-effect sensors as rotary encoders for the motors a permanent magnet is attached to the shaft of the motor (before the gearbox). Whenever the magnetic field aligns with the Hall-effect sensor a voltage peak (depending on power supply) at the output can be measured. This peak triggers a function in the MCU to increment or decrement the revolution counter.

The control commands for the robot are send from a computer running. So a serial connection via the USB port is established. Either the motor speed or a target position (target revolution counter) can be controlled. The control from the computer is done

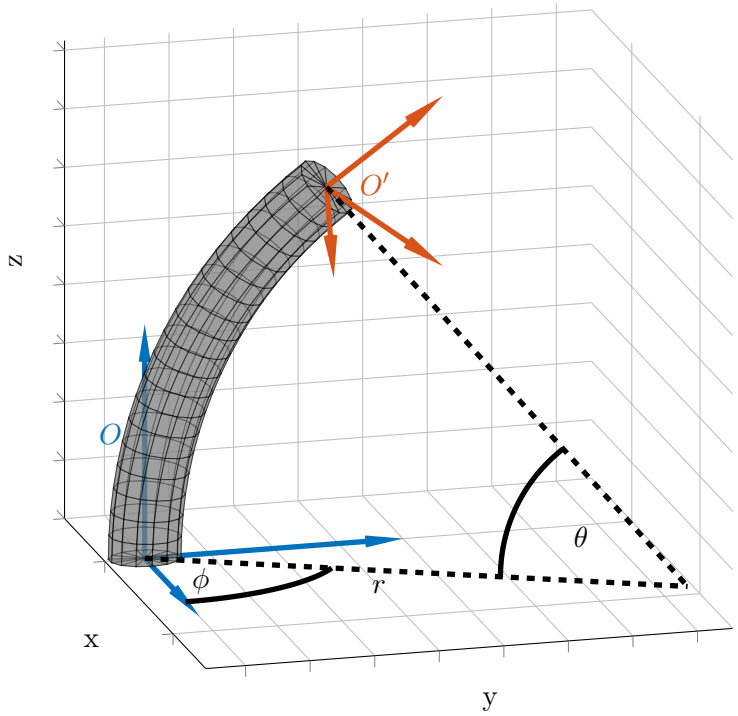


Figure 4.5: Variable nomenclature for kinematic

by sending messages with a specific identifier character via serial port. The following identifiers have been implemented:

## 4 Kinematic

The mathematical description of the robot can be split into 4 spaces. Figure 4.6 illustrates those spaces.

The configuration space describes the kinematic of the robot through the homogeneous transformation matrix. Using a constant curvature model this matrix can be defined by the mean arm length $\ell = r\theta$, the curvature $\kappa = \frac{1}{r}$ and the bending angle $\phi$. The

| ID | Message example | Response example | Description |
|---|---|---|---|
| r | *r* | *R1234.5,987.0,1000.0,500,200,1234* | This requests a sensor reading. The response consists of the 3 stretch sensors' resistances and the revolution counters. |
| s | *s.9999,.0400,-.321* | | This sets the motor speeds to the 3 values (mapped from $-1$ to 1 to $-5\,\mathrm{V}$ to $5\,\mathrm{V}$). |
| t | *t100,200,0* | | This sets the target counter to the 3 values and starts moving the motors towards them. |
| c | *c2000* | | This calibrates the Hall-sensors by pulling on every cable with the maximum force and then setting the counter value to the input value. |
| a | *a900* | | This sets all counter values to the input value (used for manual adjustments). |

Table 4.2: Commands for control via serial connection with the MCU

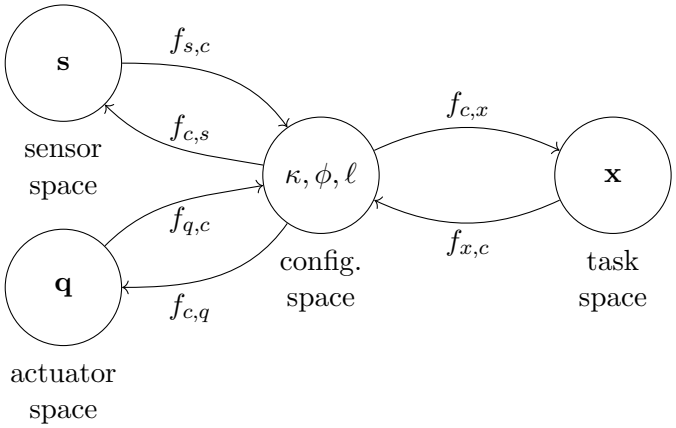


Figure 4.6: Space mapping

Rotation with the angle $\phi$ around the z-axis can be described with Equation (4.2). The transformation for the bending (in the xy-plane) is described by Equation (4.3). The transformation for the robot can then be written as product of all transformations (see Equation (4.4)). [128]

$$T_{\phi} = \begin{bmatrix} \cos\phi & \sin\phi & 0 & 0 \\ -\sin\phi & \cos\phi & 0 & 0 \\ 0 & 0 & 1 & 0 \\ 0 & 0 & 0 & 1 \end{bmatrix} \tag{4.2}$$

$$T_{r,\theta} = \begin{bmatrix} \cos\kappa\ell & 0 & -\sin\kappa\ell & r\left(1-\cos\kappa\ell\right) \\ 0 & 1 & 0 & 0 \\ \sin\kappa\ell & 0 & \cos\kappa\ell & r\sin\kappa\ell \\ 0 & 0 & 0 & 1 \end{bmatrix} \tag{4.3}$$

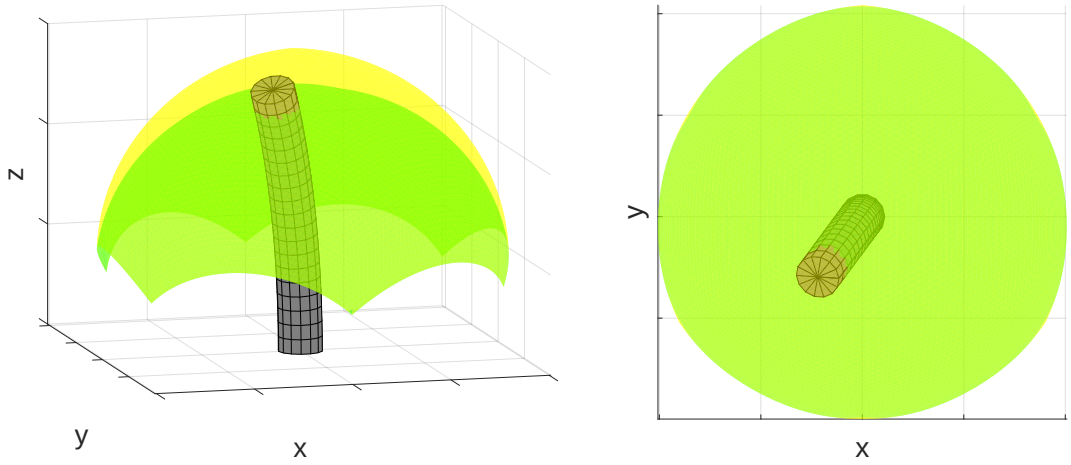


(a) 3D view of the task space (b) 2D view of the task space

Figure 4.7: Task space

$$T(\kappa,\phi,\ell) = T_{\phi}T_{r,\theta} = \begin{bmatrix} \cos\phi\cos\kappa\ell & \sin\phi & -\cos\phi\sin\kappa\ell & \frac{\cos\phi(1-\cos\kappa\ell)}{\kappa} \\ -\sin\phi\cos\kappa\ell & \cos\phi & \sin\phi\sin\kappa\ell & \frac{\sin\phi(\cos\kappa\ell-1)}{\kappa} \\ \sin\kappa\ell & 0 & \cos\kappa\ell & \frac{\sin\kappa\ell}{\kappa} \\ 0 & 0 & 0 & 1 \end{bmatrix} \tag{4.4}$$

The task space is the space in which the end-effector moves. It is defined by 3 spacial coordinates $(x, y, z)$. Assuming the motors are not operating at their force maximum, the tendon lengths lie in a constant range. The task space for this case is visualized in Figure 4.7.

For the mapping from the configuration space to the task space $f_{c,x}$ only the last

column of the transformation matrix is required (see Equations (4.5) to (4.7)). [128]

$$x = \frac{\cos\phi\,(1 - \cos\kappa\ell)}{\kappa} \tag{4.5}$$

$$y = \frac{\sin\phi\,(\cos\kappa\ell - 1)}{\kappa} \tag{4.6}$$

$$z = \frac{\sin\kappa\ell}{\kappa} \tag{4.7}$$

For the transformation from the task space to the configuration space $f_{x,c}$ those equations can be solved for the configuration variables (see Equations (4.8) to (4.10)). [128]

$$\kappa = \frac{2\sqrt{x^2 + y^2}}{x^2 + y^2 + z^2} \tag{4.8}$$

$$\phi = \operatorname{atan2}(y, x) \tag{4.9}$$

$$\ell = \frac{1}{\kappa}\arcsin(z\kappa) \tag{4.10}$$

The actuator space $\mathbf{q}$ consists of the 3 cable lengths $(l_1, l_2, l_3)$. As those actuators are linear independent, a closed form mapping from actuator space to configuration space $f_{s,c}$ exists. With $\varphi_1 = \frac{1}{2}\pi$, $\varphi_2 = \frac{7}{6}\pi$ and $\varphi_3 = \frac{11}{6}\pi$ those equations are shown in

Equations (4.11) to (4.13)). [128]

$$\kappa = \frac{2\sqrt{l_1^2 + l_2^2 + l_3^2 - l_1 l_2 - l_1 l_3 - l_2 l_3}}{\delta\left(l_1 + l_2 + l_3\right)} \tag{4.11}$$

$$\phi = \operatorname{atan2}\left(l_2 + l_3 - 2l_1, \sqrt{3}\left(l_2 - l_3\right)\right) \tag{4.12}$$

$$\ell = \frac{l_1 + l_2 + l_3}{3} \tag{4.13}$$

The mapping from configuration space to actuator space $f_{c,q}$ can be described with Equation (4.14). [128]

$$l_i = \ell\left(1 - \kappa\delta\cos\left(\varphi_i - \phi\right)\right) \tag{4.14}$$

The sensor space consists of the 3 sensor lengths $(s_1, s_2, s_3)$. As the sensor are rotated by 30° to the cables, the equations for the mapping between sensor space and configuration space ($f_{s,c}$ and $f_{c,s}$, see Equations (4.15) to (4.18)) look similar to the mapping between actuator space and configuration space. [128]

$$\kappa = \frac{2\sqrt{s_1^2 + s_2^2 + s_3^2 - s_1 s_2 - s_1 s_3 - s_2 s_3}}{\delta\left(s_1 + s_2 + s_3\right)} \tag{4.15}$$

$$\phi = \text{atan2}\left(s_2 + s_3 - 2s_1, \sqrt{3}\left(s_2 - s_3\right)\right) - \frac{\pi}{6} \tag{4.16}$$

$$\ell = \frac{s_1 + s_2 + s_3}{3} \tag{4.17}$$

$$s_i = \ell\left(1 - \kappa\delta\cos\left(\alpha_i - \phi\right)\right) \tag{4.18}$$

A more general mathematical model that does not assume the cables and sensors to be evenly distributed is shown in Appendix A.

## 5 Material Characterization

[33] used a conductive textile (Electrolycra, from Mindsets Ltd, United Kingdom) which is efficient for strain levels up to 30 %. For the mentioned conductive textile curves, the resistance does not change beyond 30 % of the engineering strain. On the other hand, rubber bands can work effectively for 10 unitcommands times higher strain levels (up to 300 % strain levels).

For using the Ecoflex 00-30 elastomer as a body of the soft robotic arm and also intensively studying the rubber band, the following things are really important for us. Tensile test (stress-strain constitutive relation), Resistance-tension (Resistance- Strain curve) Cyclic tensile test (Mechanical Hysteresis behavior), Resistance cyclic test (Resistance cyclic test).

Material testing has been done following the instruction from ASTM D412 - 16) Standard Test Methods for Vulcanized Rubber and Thermoplastic Elastomers—Tension( . First, using 3d printing and rapid prototyping techniques the mold for the tensile specimens has been made. The specimens made by degassing the liquid mixture of the elastomer in vacuum, following up with a 2 h to 3 h of curing time. Mullin effects has been removed by stretching the specimen for several times. The dimension for elastomer specimen is $4.2\,\text{mm} \times 12\,\text{mm} \times 35.88\,\text{mm}$. The rate of the experiment (i.e. the strain rate) was set to be 60 mm/min. We also tried higher speed (e.g. 200 mm/min) and we did not observe significant strain rate sensitivity, which is also in agreement with the

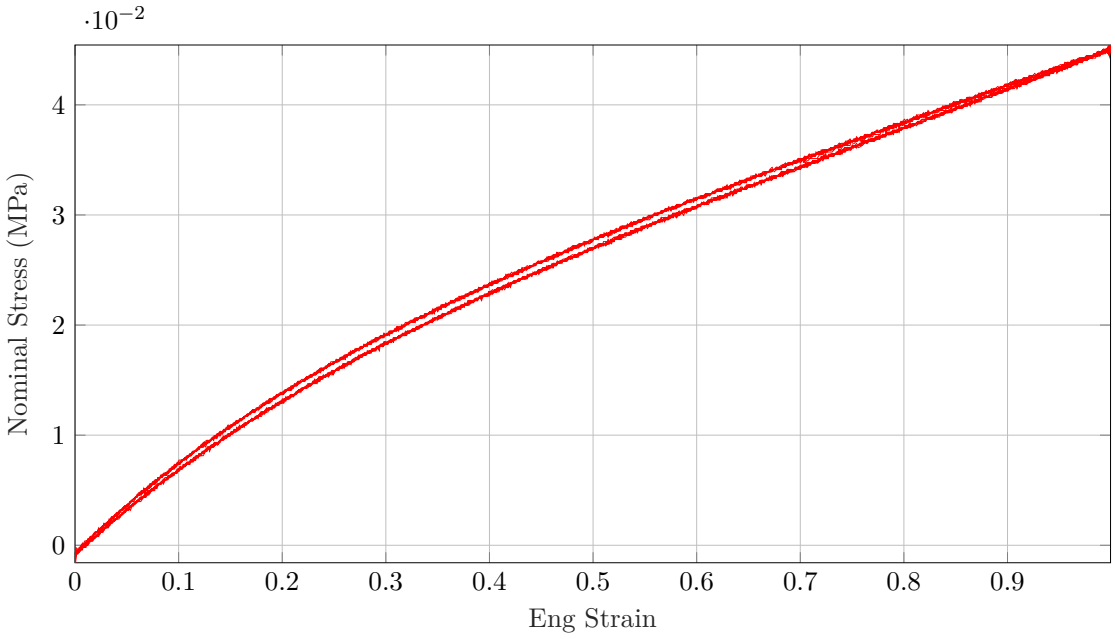


Figure 5.1: Cyclic stress- strain curve for the Ecoflex 00-30 which shows negligible hystesis.

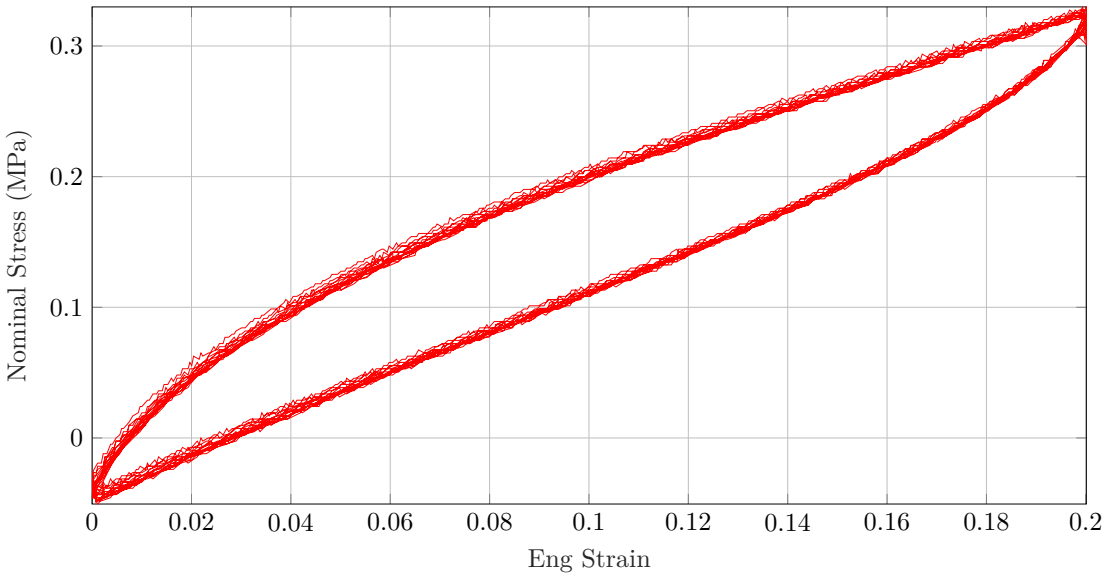


Figure 5.2: Cyclic stress- strain curve for the conductive rubber cord [2] which shows significant hystesis effect.

literature, as reported by the [88]. They reported that there is less than 3 % viscoelastic effect for Eco-flex 00-30. The test stand used for the material testing experiment is Mark 10, ESM 303 (C.S.C Force Measurement, Inc.).

Figure 5.2 shows the cyclic stress -strain loading curve for the rubber band for 20 cycles. We observe a significant hysteresis effect on this curve. Therefore we observe a large phase difference between the stress and the strain. Here if we denote the area under the loading curve (upper curves) by and denote the area for the unloading curve (lower curves) by . We can compute the dissaptive energy compare to the unloading curve which is equal to 59.99 %. In addition to hystesis effect we can also observe the stress/force relaxation effect. As we notice a band width for the upper curve and the

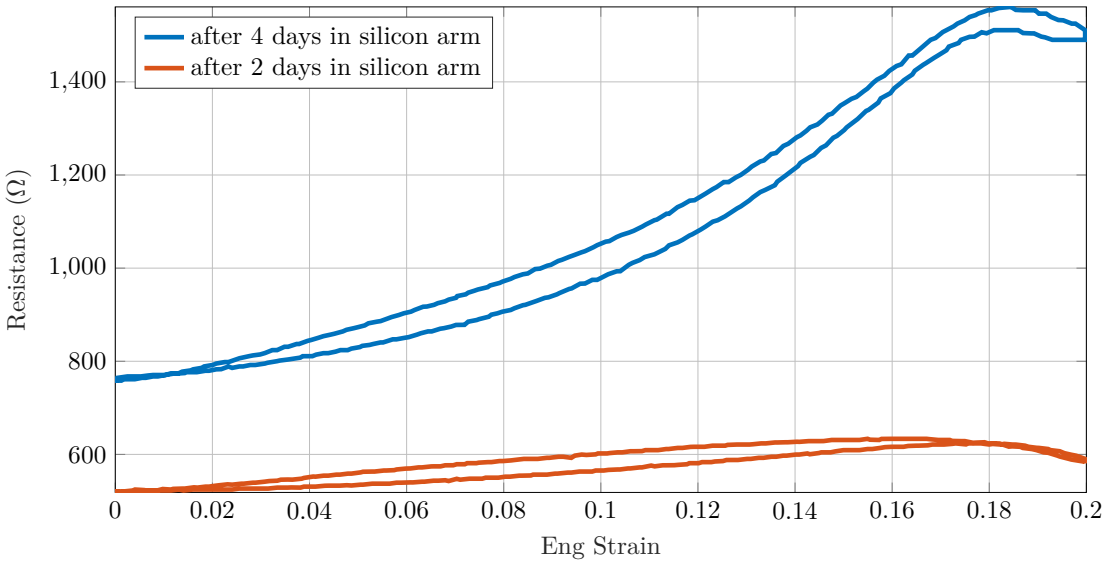


Figure 5.3: Steady Resistance- strain curve for the conductive rubber band [2] up to 20 % engineering strain. which shows significant aging effect.

lower curve in Fig2. Meaning, during the experiment by repeating the cycles the plot has a shift to the below.

In Figure 5.3 we show the experimental result for the aging effect of the rubber band. By aging here we mean the life of the rubber band inside the elastomeric arm. We noticed a different behaviour for the aged rubber bands. Due to diffusivity of the silicone rubber particles into the rubber band the rubber resistance will increase on a timely manner. The blue curve (top curve) is the rubber band resistance after 2 days, which shows two to three order of magnitude increase in resistant. However, it also changes the behavior of the material for the strains beyond 17 % and we do not onbserve the twist anymore. After runing several experiments, the data from the aged rubber band has been more

useful in terms of calibrating the sensors. Further research should account for the tuning and regulating the rubber bands resistance and its sensitivity to the enviorment.

For measuring the real-time resistance of the conductive rubber, an Arduino UNO microcontroller was utilized and programmed using MATLAB Arduino package. Wires for measuring the real-time resistance were attached close to the edge of the tensile stand's grippers. Resistance data aquisation has been synchronized with the displacement data from the tensile experiment.

# 6 Robot Control

This section describes the robot control. First a calibration process for the robot is presented. In the next steps the robot is tested in an open-loop and an closed-loop environment.

## 6 Calibration

Because the behavior of the conductive rubber bands doesn't follow a linear pattern the robot is calibrated before every experiment. During this calibration process multiple data points are collected with their respective length (obtained from EM-senors). For those points a polynomial of 3rd order is fitted and used to convert from sensor reading to sensor length. The calibration algorithm is shown in Algorithm 2. Figure 6.1 shows the sensor readings and the sensor length during the calibration process. The data shows that the resistance of the peaks decreases over time. The biggest change of the resistance range happens during the first cycle. To get more consistent data for the calibration, the first cycle is cut off and thereby not used for the calibration. This cycle shows significantly different results due to the Mullins effect. Figure 6.2 shows the polynomial regression for those data points. Even though all sensors function in a different resistance range, the basic shape of the data matches.

**Algorithm 2:** calibration process

**Input:** max values $c_{max}$
**Input:** number of steps $N_{steps}$
**Input:** number of cycles $N_{cycles}$
**Result:** polynomial regression function for each sensor $s_i(R_{si})$

**for** $n_c \leftarrow 0$ **to** $N_{cycles}$ **by** 1 **do**
  **for** $c \leftarrow c_{max}$ **to** 0 **by** $\frac{1}{N_{steps}}$ **do**
    move motors to counter position $c$;
    read sensor resistances $R_{si}$;
    read robot length using EM sensor $\ell_i$;
  **end**
  **for** $c \leftarrow 0$ **to** $c_{max}$ **by** $\frac{1}{N_{steps}}$ **do**
    move motors to counter position $c$;
    read sensor resistances $R_{si}$;
    read robot length using EM sensor $\ell_i$;
  **end**
**end**
calculate polynomial regression for data of each sensor $s_i\,(R_{si})$;

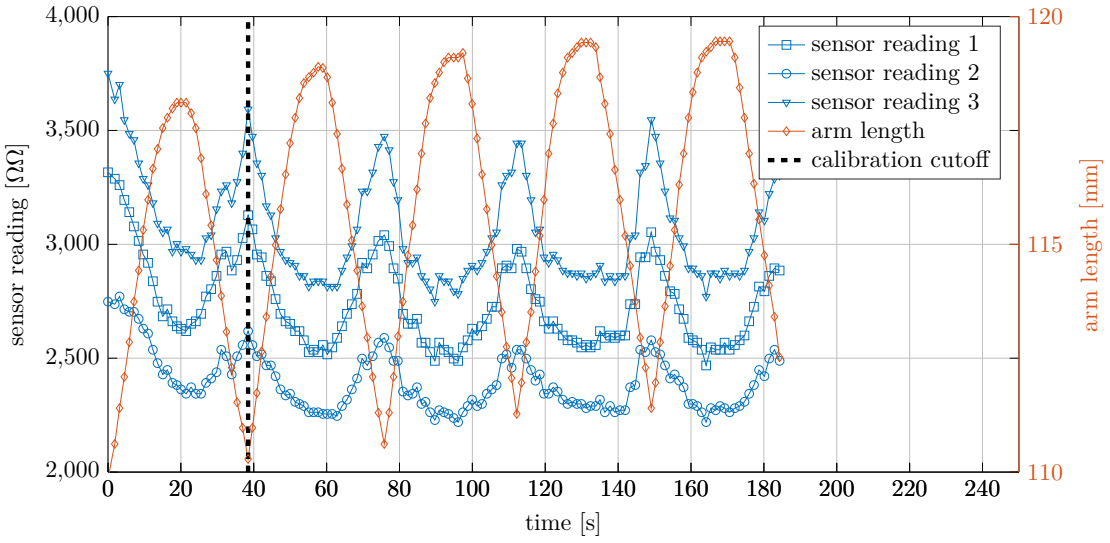


Figure 6.1: Calibration process

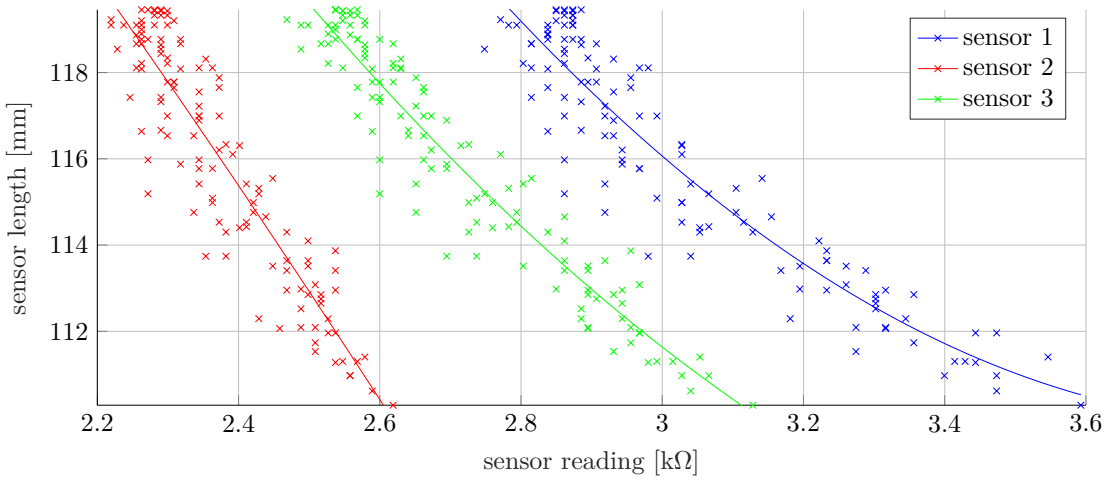


Figure 6.2: 3rd Order regression of calibration data

## 6 Open-Loop Control

To test the open-loop behavior of the robot a circular trajectory was discretized at to a number of points. First the robot undergoes a calibration step to set the initial state to a known position. During this calibration the motors pull on every cable with the equal maximum force and after that release all cables equally. The end-effector is then moved to the predefined trajectory points by pulling and releasing the cables to the required lengths (calculated with the inverse kinematic).

Figure 6.3 shows the robot at different points along the experiment. The end-effector coordinates acquired from the Hall effect sensors, EM sensor and the stretch sensors are shown in Figure 6.4. Figure 6.5 presents the same data over time.

The Figures 6.4 and 6.5 show that the basic shape of the trajectory can be recon-

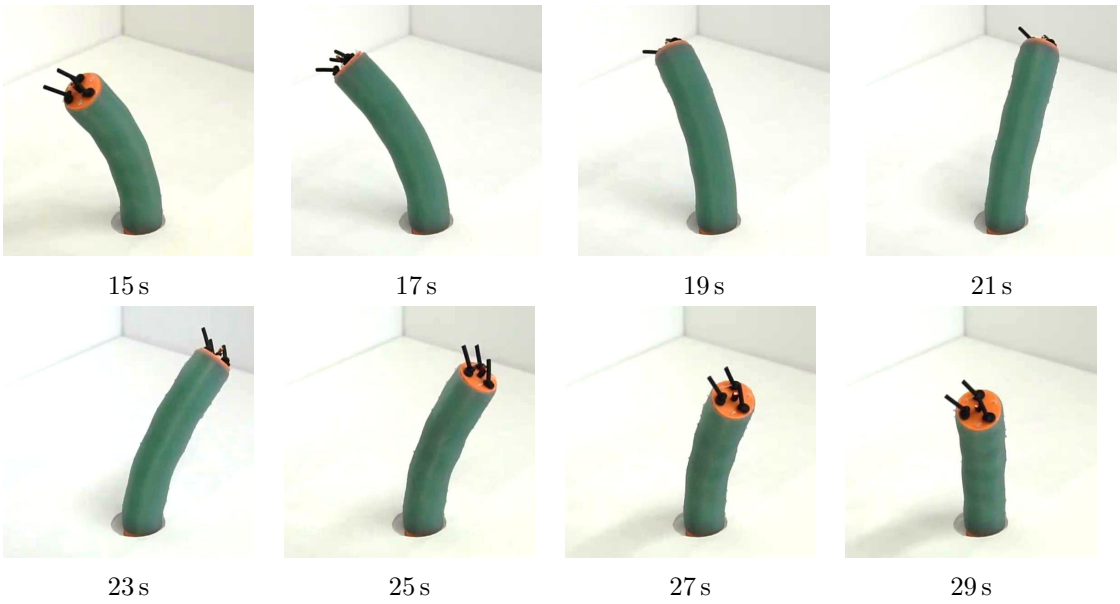


Figure 6.3: Open-loop recording

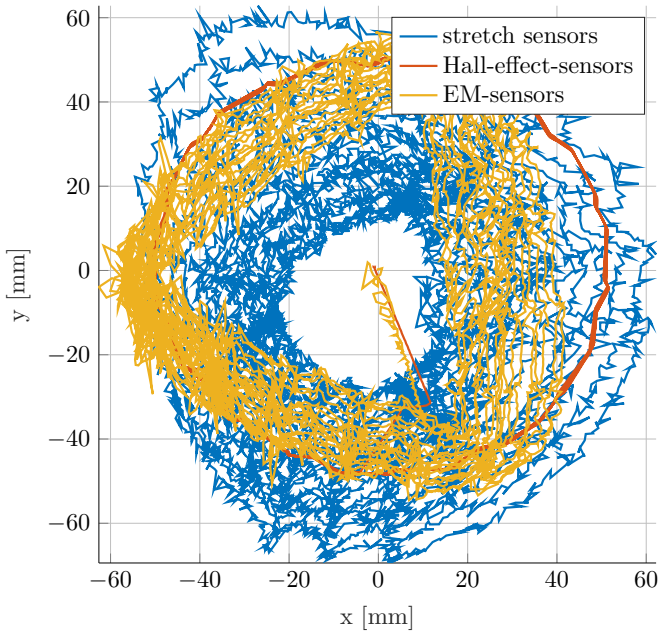


Figure 6.4: Open-loop end-effector coordinates

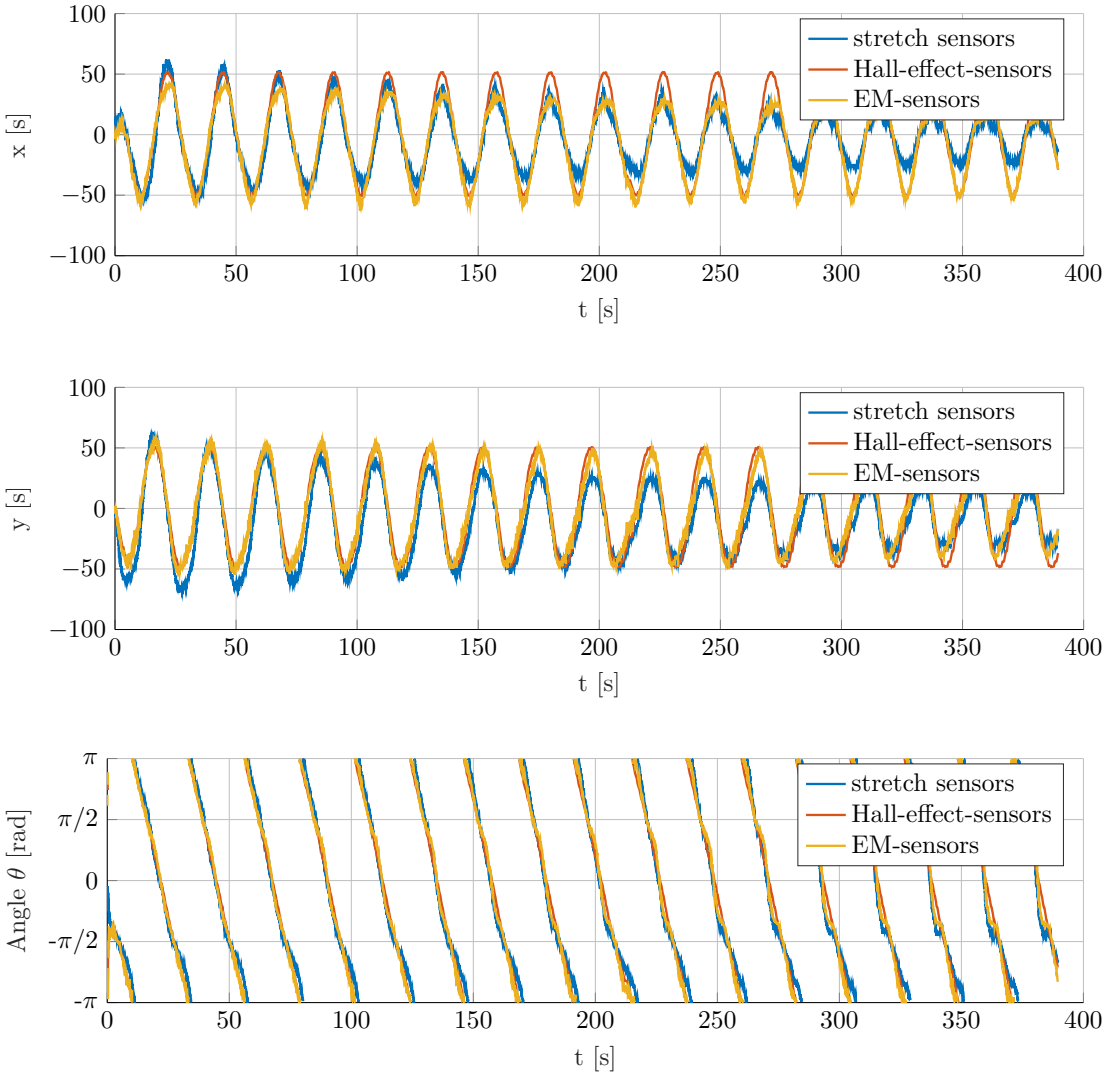


Figure 6.5: Open-loop end-effector coordinates over time

structed. However the data in Figure 6.5 shows that with increasing time the amplitude of the stretch sensors decreases in the same way as observed during the tensile testing (Section 5). Despite this fact the direction toward which the arm is bending still matches the direction obtained from the stretch sensors.

Also it can be observed that the x coordinate of the trajectory does not reach the expected position. The reason for that may be friction forces between the cable located at $(-r_{cable}, 0)^T$ and robot. Even though the motor releases the cable by the right amount the friction prevents the arm to reach the desired position. Using lubrication could reduce the friction. However as the stretch sensors are very sensitive to silicon based liquids, lubrication the arm was avoided.

## 6 Closed-Loop Control

In this section the stretch sensors are used in a closed-loop control to actuate the robot to a defined target. In this experiment a PI-controller was used. A low pass filter (moving average filter) was implemented to remove high frequency noise of the sensor readings. The controller setup is shown in Figure 6.6. Here $r(t)$ is the target cable length, $u(t)$ is the speed input for the DC motor and $y(t)$ is the cable length calculated from the sensor reading. For simplification only one motor was actuated.

Figure 6.7 shows some frames of the experiment.

Figure 6.8 shows the results of this experiment. The data obtained from the stretch sensors can be used to control the robot to specified position. However the viscoelastic

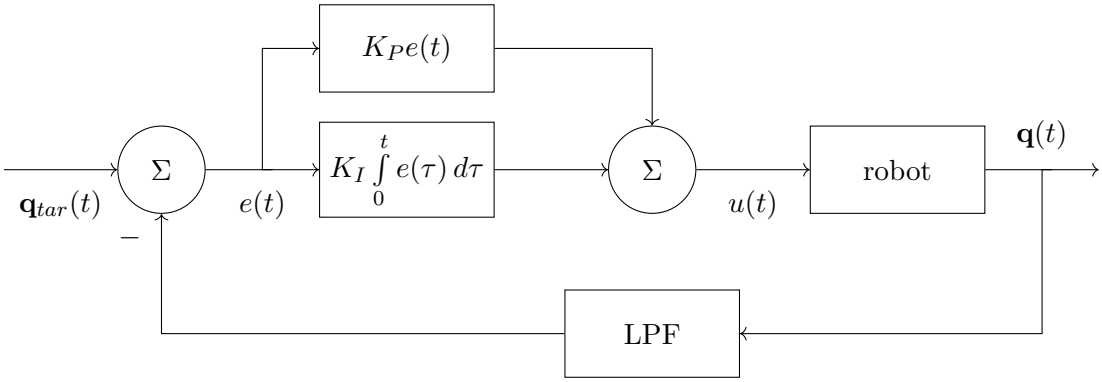


Figure 6.6: PI controller

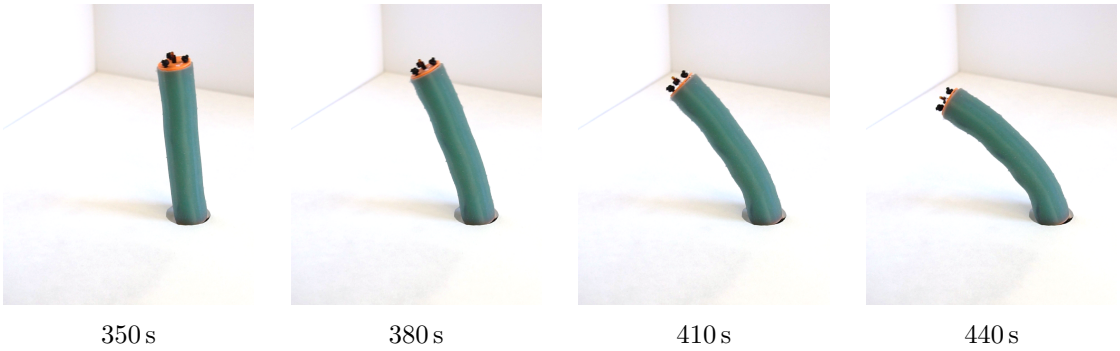


Figure 6.7: Closed-loop recording

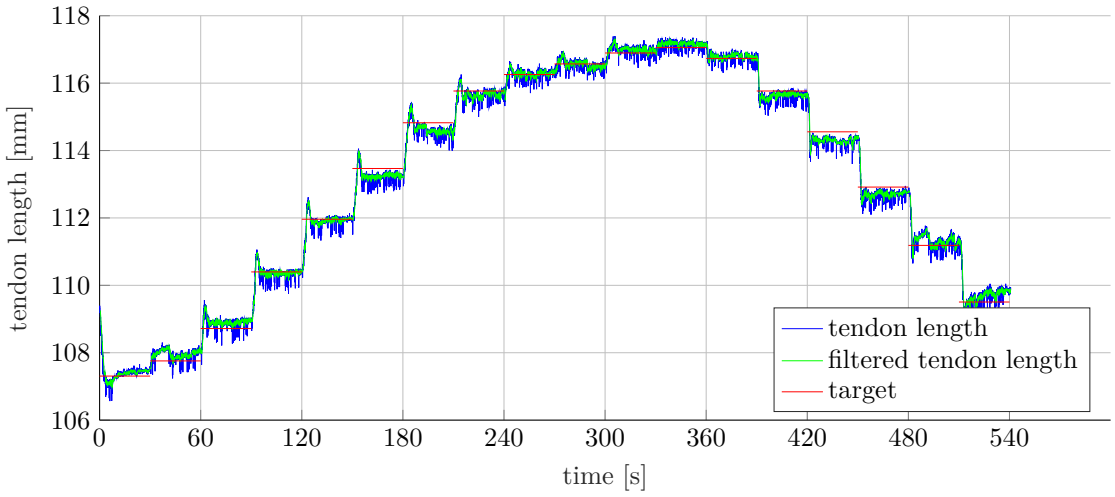


Figure 6.8: Closed-loop cable length

properties of those sensors make it difficult to actuate the robot fast, as in those cases the sensors become inaccurate or require taking the viscoelastic behavior into account.

# 7 Conclusion and Outlook

Soft continuum robotic arms, which combine the dexterity and high degree of freedom of continuum robots, are able to escape many of the pitfalls of their rigid and hard continuum counterparts due to their use of hyperelastic materials [110], and better mimic the gentleness, articulation, and high level of control and haptic ability found in nature. Due to the low-stiffness and light-weight materials, much of the power demand seen with conventional rigid or continuum hard robots is unnecessary, allowing for the use of batteries and small DC motors to provide the motive force for actuation. It is because of this that soft continuum robots prove to be exceptional candidates for modular design, whereby each module contains its own source of actuation and control, making it possible to design extendable and/or more highly complex soft robotic arms with unique functionalities.

Using carbon impregnated rubber cords as stretch sensors to sense the current state of a soft robot presents a lot potential as material properties of the soft robot are not required for the kinematic model. However those stretch sensors bring many challenges along. It is hard to maintain consistent results over longer periods of time due to high environmental dependencies of the sensors, which makes calibration before usage unavoidable. That aside even within a single experiment consistency is not guaranteed. A more accurate model of the stretch sensors including their hysteresis effect would be needed.

As the created robot uses small actuators and electronic parts this design is suited to

be extended to a multi-section robot. As the robot would be able to carry the weight of its hardware, those parts could be combined in a small module that is connected wireless (over an HTTP server) to a computer that gives control commands. A robot like this could have many different applications as it is easy extendable by adding more sections.

# A General Mathematical Model

## Forward Kinematic

For the kinematic a constant curvature model is assumed. The length of a thread along the robot is therefor only dependent on the distance to the bending axis. The function $L(X, Y)$ describes this length for any thread. The equipotential curves (curves of constant value) are lines parallel to the bending axis.

The length $L(R)$ of a thread with distance $R$ to the bending axis can be calculated using Equation (A.1).

$$L(R) = R\theta \tag{A.1}$$

Because the length $L$ is linear proportional to the distance $R$, the function $L(X, Y)$ has to be a plane.

$$L(X, Y) = a_1 + a_2 X + a_3 Y \tag{A.2}$$

With the known sensor length the coefficients $a_i$ can be calculated by solving the following linear system of equations:

$$\begin{bmatrix} 1 & X_{s1} & Y_{s1} \\ 1 & X_{s2} & Y_{s2} \\ 1 & X_{s3} & Y_{s3} \end{bmatrix} \begin{bmatrix} a_1 \\ a_2 \\ a_3 \end{bmatrix} = \begin{bmatrix} s_1 \\ s_2 \\ s_3 \end{bmatrix} \tag{A.3}$$

The gradient of the function $\nabla L(X, Y)$ gives the direction $\vec{n}$ toward which the arm is

bending.

$$\nabla L\left(X,Y\right) = \begin{bmatrix} a_2 \\ \\ a_3 \end{bmatrix} \tag{A.4}$$

$$\left\|\nabla L\left(X,Y\right)\right\| = \vec{n} \tag{A.5}$$

For $\vec{n} \neq \vec{0}$ the arm is bend. To determine the bending angle $\phi$ and the bending radius $R(\vec{0}) = r$ of a line going through the center of the arm, two length values $L(\vec{0})$ and $L(\vec{n})$ are used. With Equation (A.6) the values $\phi$ and $r$ can be calculated.

$$\phi = \frac{L(\vec{0})}{R} = \frac{L(\vec{n})}{R(\vec{n})} \tag{A.6}$$

$$r = \frac{L(\vec{n})}{L(\vec{0}) - L(\vec{n})} \tag{A.7}$$

$$\phi = \frac{L(\vec{0})\left(L(\vec{0}) - L(\vec{n})\right)}{L(\vec{n})} \tag{A.8}$$

Assuming the arm only bends in the x-z-plane, the end-effector position can be calcu-

lated with the homogeneous transformation in Equation A.9

$$T_{r,\theta} = \begin{bmatrix} \cos\theta & 0 & -\sin\theta & r\,(1-\cos\theta) \\ 0 & 1 & 0 & 0 \\ \sin\theta & 0 & \cos\theta & r\sin\theta \\ 0 & 0 & 0 & 1 \end{bmatrix} \tag{A.9}$$

To get the actual end-effector position a rotation to the bending direction has to added:

$$\phi = \operatorname{atan2}(n_y, n_x) \tag{A.10}$$

$$T_{\phi} = \begin{bmatrix} \cos\phi & \sin\phi & 0 & 0 \\ -\sin\phi & \cos\phi & 0 & 0 \\ 0 & 0 & 1 & 0 \\ 0 & 0 & 0 & 1 \end{bmatrix} \tag{A.11}$$

The combined transformation matrix from the base to the end-effector is then dependent on $\phi$, $\theta$ and $r$:

$$T(\phi, \theta, R) = T_{\phi} T_{r,\theta} \tag{A.12}$$

**Inverse Kinematic**

For the inverse kinematics the position of the end effector $\vec{p}$ is known and the cable length is determined. In the first step the direction in which the arm bends is calculated. This is done by projecting the vector $\begin{bmatrix} x & y & z \end{bmatrix}^\intercal$ onto the xy plane. Equation (A.13) shows the bending direction vector in a normalized form.

$$\vec{n} = \begin{bmatrix} n_x \\ \\ n_y \end{bmatrix} = \frac{1}{\sqrt{x^2 + y^2}} \begin{bmatrix} x \\ \\ y \end{bmatrix} \tag{A.13}$$

The end effector position is then rotated to the x-z-plane:

$$\vec{p} = T_2^{-1} \begin{pmatrix} x & y & z \end{pmatrix}^\intercal \tag{A.14}$$

Using the translational part of Equation (A.9) the radius $r$ and the angle $\theta$ can be calculated (see Equations (A.15) and (A.16)).

$$(p_x - r)^2 + p_z^2 = r^2 \left(\cos^2\theta + \sin^2\theta\right) = r^2 \Rightarrow r = \frac{p_x^2 + p_z^2}{2p_x} \tag{A.15}$$

$$p_z = r \sin\theta \Rightarrow \theta = \arcsin \frac{2p_x p_z}{p_x^2 + p_z^2} \tag{A.16}$$

To obtain the cable length the radii for the cables $r_{ci}$ are required. The radii can be

calculated by projecting the coordinates of the cables $\begin{bmatrix} x_{ci} & y_{ci} \end{bmatrix}^\intercal$ (x and y at the base of the arm) onto the bending direction vector $\vec{n}$. The length of the component along $\vec{n}$ is the subtracted from $r$ to obtain the radius for a cable $r_{ci}$ (see Equation (A.17)).

$$r_{ci} = r - \frac{\begin{bmatrix} x_{ci} & y_{ci} \end{bmatrix} \cdot \vec{n}}{\|\vec{n}\|^2} \tag{A.17}$$

Using Equation (A.18) the length for an cable can then be calculated.

$$L\left(x_{ci}, y_{ci}\right) = r_{ci}\theta \tag{A.18}$$

## B Code Instructions

The code that is flashed on the MCU expects a hardware setup as shown in Figure 4.4. If changes are made the pin numbers have to be updated in the Arduino code ("Arm.cpp" and "main.ino").

Flowcharts for the matlab codes are given in Figures B.1 to B.5. Other files may be required but are self explanatory such as "rotx.m" which returns a rotation matrix around the x-Axis.

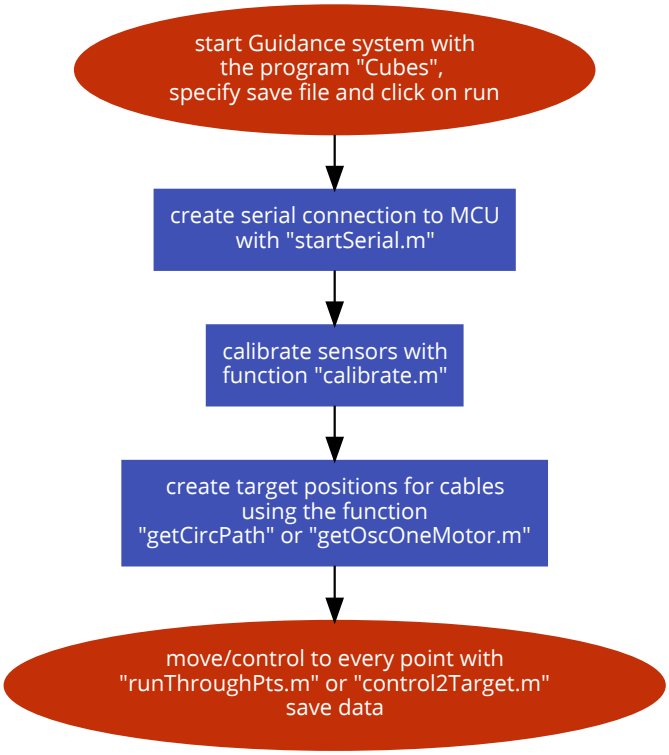


Figure B.1: experiment steps

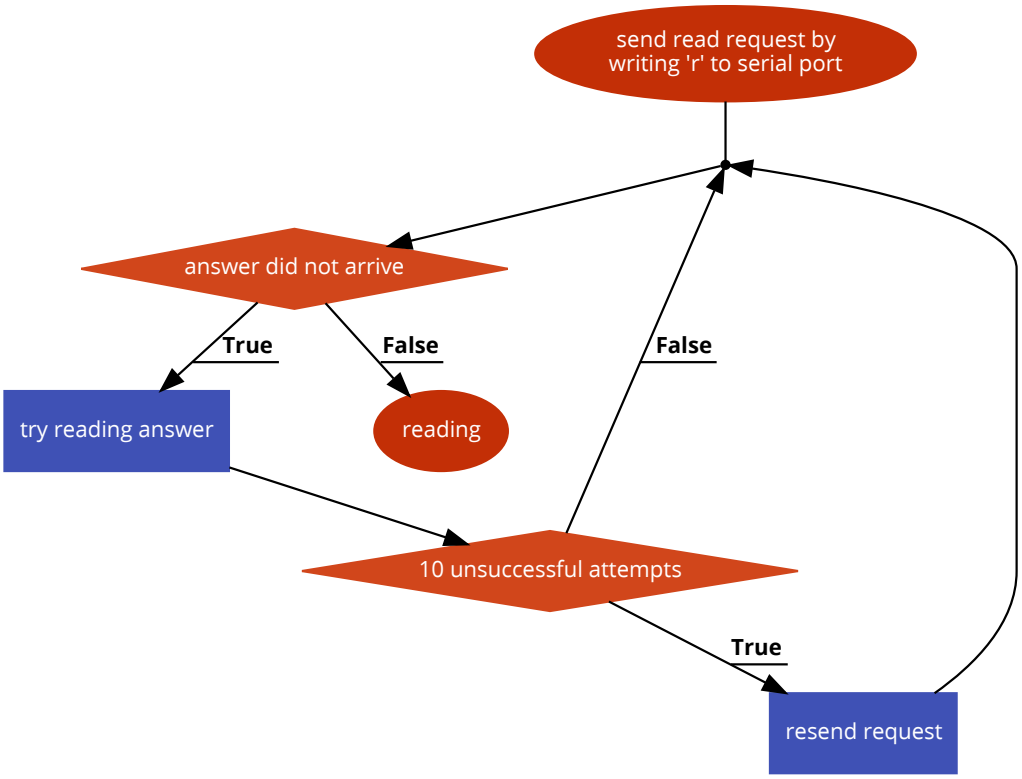


Figure B.2: flow chart for “readSensors.m”

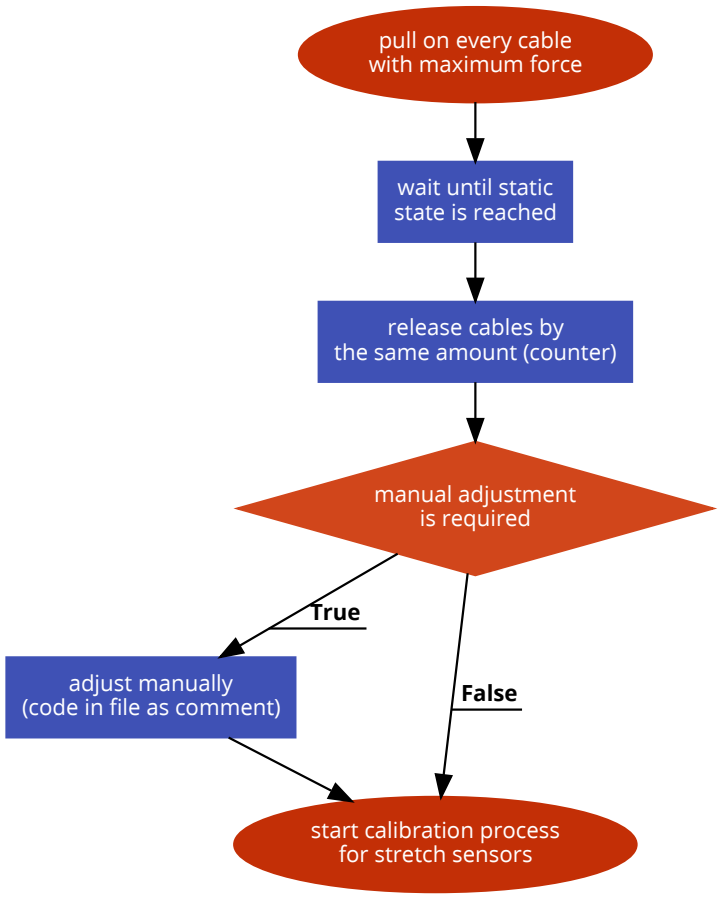


Figure B.3: flow chart for “calibration.m”

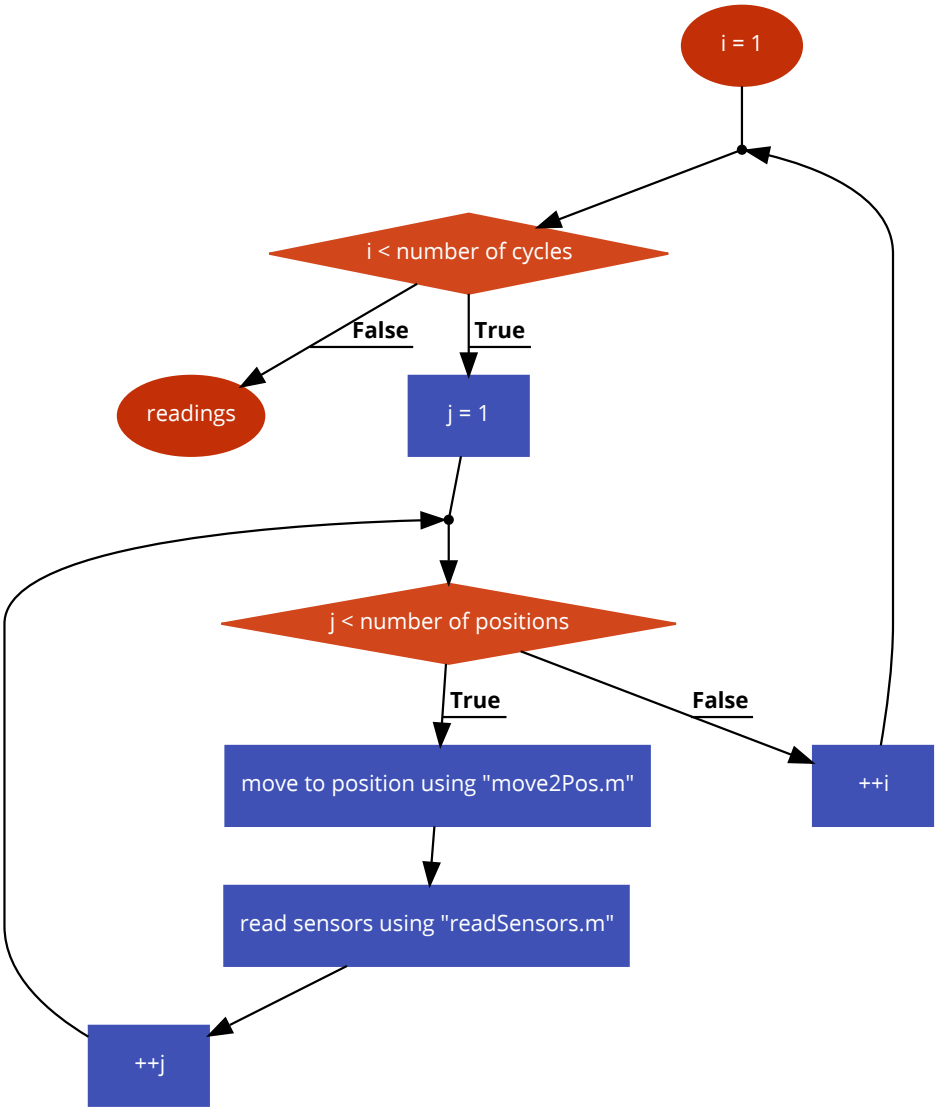


Figure B.4: flow chart for “runThroughPts.m”

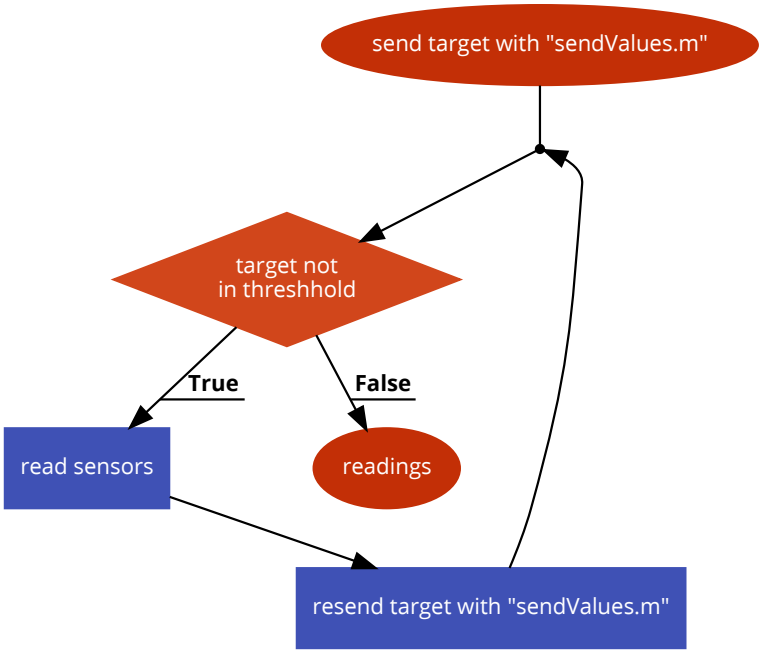


Figure B.5: flow chart for “move2Pos.m”

## Bibliography


[1] Haider Abidi, Giada Gerboni, Margherita Brancadoro, Jan Fras, Alessandro Diodato, Matteo Cianchetti, Helge Wurdemann, Kaspar Althoefer, and Arianna Menciassi. Highly dexterous 2-module soft robot for intra-organ navigation in minimally invasive surgery. *International Journal of Medical Robotics and Computer Assisted Surgery*, 14(1), 2018.

[2] Adafruit. Conductive rubber cords stretch sensor.

[3] John Amend, Nadia Cheng, Sami Fakhouri, and Bill Culley. Soft Robotics Commercialization: Jamming Grippers from Research to Product. *Soft Robotics*, 3(4):213–222, 2016.

[4] John R. Amend, Eric Brown, Nicholas Rodenberg, Heinrich M. Jaeger, and Hod Lipson. A positive pressure universal gripper based on the jamming of granular material. *IEEE Transactions on Robotics*, 28(2):341–350, 2012.

[5] Yasmin Ansari, Egidio Falotico, Yoan Mollard, Baptiste Busch, Matteo Cianchetti, and Cecilia Laschi. A Multiagent Reinforcement Learning approach for inverse kinematics of high dimensional manipulators with precision positioning. *2016 6th IEEE International Conference on Biomedical Robotics and Biomechatronics (BioRob)*, pages 457–463, 2016.

[6] Arduino. ARDUINO PRO MINI.

[7] Arduino. Arduino Uno SMD.

[8] Alberto Arezzo, Yoav Mintz, Marco Ettore Allaix, Simone Arolfo, Marco Bonino, Giada Gerboni, Margherita Brancadoro, Matteo Cianchetti, Arianna Menciassi, Helge Wurdemann, Yohan Noh, Kaspar Althoefer, Jan Fras, Jakob Glowka, Zbigniew Nawrat, Gavin Cassidy, Rich Walker, and Mario Morino. Total mesorectal excision using a soft and flexible robotic arm: a feasibility study in cadaver models. *Surgical Endoscopy and Other Interventional Techniques*, 31(1):264–273, 2017.

[9] Yan Bailly and Yacine Amirat. Modeling and control of a hybrid continuum active catheter for aortic aneurysm treatment. *Proceedings - IEEE International Conference on Robotics and Automation*, 2005(April):924–929, 2005.

[10] Andrea Bajo and Nabil Simaan. Hybrid motion/force control of multi-backbone continuum robots. *International Journal of Robotics Research*, 35(4):422–434, 2016.

[11] Daniel R. Baker and Charles W. Wampler. On the Inverse Kinematics of Redundant Manipulators. *The International Journal of Robotics Research*, 7(2):3–21, 1988.

[12] Circuit Basics. Ohm Meter.

[13] Charles M. Best, Morgan T. Gillespie, Phillip Hyatt, Levi Rupert, Vallan Sherrod, and Marc D. Killpack. A New Soft Robot Control Method: Using Model Predictive

Control for a Pneumatically Actuated Humanoid. *IEEE Robotics & Automation Magazine*, 23(3):75–84, 2016.

[14] Botond Bócsi, Duy Nguyen-Tuong, Lehel Csató, Bernhard Schölkopf, and Jan Peters. Learning inverse kinematics with structured prediction. *IEEE International Conference on Intelligent Robots and Systems*, pages 698–703, 2011.

[15] Julien Bosman, Thor Morales Bieze, Othman Lakhal, Mario Sanz, Rochdi Merzouki, and Christian Duriez. Domain decomposition approach for FEM quasistatic modeling and control of Continuum Robots with rigid vertebras Do- main decomposition approach for FEM quasistatic modeling and control of Continuum Robots with rigid vertebras. *IEEE International Conference on Robotics and Automation*, (May):4373–4378, 2015.

[16] David Braganza, Darren M. Dawson, Ian D. Walker, and Nitendra Nath. A neural network controller for continuum robots. *IEEE Transactions on Robotics*, 23(6):1270–1277, 2007.

[17] David T. Branson, Robgjie Kang, Emanuele Guglielmono, and Darwin G. Caldwell. Control architecture for robots with continuum arms inspired by Octopus vulgaris neurophysiology. *Proceedings - IEEE International Conference on Robotics and Automation*, pages 5283–5288, 2012.

[18] L. Bruzzone and G. Quaglia. Review article: locomotion systems for ground mobile robots in unstructured environments. *Mechanical Sciences*, 3(2):49–62, 2012.

[19] Jessica Burgner-Kahrs, D. Caleb Rucker, and Howie Choset. Continuum Robots for Medical Applications: A Survey, 2015.

[20] D. Caleb Rucker and Robert J. Webster. Mechanics of continuum robots with external loading and general tendon routing. *Springer Tracts in Advanced Robotics*, 79(6):645–654, 2014.

[21] M. Calisti, F. Corucci, A. Arienti, and C. Laschi. Dynamics of underwater legged locomotion: Modeling and experiments on an octopus-inspired robot. *Bioinspiration and Biomimetics*, 10(4):46012, 2015.

[22] M. Calisti, M. Giorelli, G. Levy, B. Mazzolai, B. Hochner, C. Laschi, and P. Dario. An octopus-bioinspired solution to movement and manipulation for soft robots. *Bioinspiration and Biomimetics*, 6(3), 2011.

[23] Marcello Calisti, Egidio Falotico, and Cecilia Laschi. Hopping on Uneven Terrains with an Underwater One-Legged Robot. *IEEE Robotics and Automation Letters*, 1(1):461–468, 2016.

[24] D Camarillo, C Milne, C Carlson, M Zinn, and J Salisbury. Mechanics modeling of tendon driven continuum manipulators. *IEEE Trans. Robot*, vol(6):24no6pp1262–1273, 2008.

[25] David B. Camarillo, Christopher R. Carlson, and J. Kenneth Salisbury. Task-Space Control of Continuum Manipulators with Coupled Tendon Drive. *Springer Tracts in Advanced Robotics*, 54(4):271–280, 2009.

[26] David B. Camarillo, Kevin E. Loewke, Christopher R. Carlson, and J. Kenneth Salisbury. Vision based 3-D shape sensing of flexible manipulators. *Proceedings - IEEE International Conference on Robotics and Automation*, pages 2940–2947, 2008.

[27] G. Chen, M. T. Pham, and T. Redarce. Sensor-based guidance control of a continuum robot for a semi-autonomous colonoscopy. *Robotics and Autonomous Systems*, 57(6-7):712–722, 2009.

[28] Qiyi Chen, Peng Fei Cao, and Rigoberto C. Advincula. Mechanically Robust, Ultraelastic Hierarchical Foam with Tunable Properties via 3D Printing. *Advanced Functional Materials*, 1800631:1–9, 2018.

[29] Yang Chen, Shaofei Guo, Cunfeng Li, Hui Yang, and Lina Hao. Size recognition and adaptive grasping using an integration of actuating and sensing soft pneumatic gripper. *Robotics and Autonomous Systems*, 104:14–24, 2018.

[30] Gregory S. Chirikjian and Joel W. Burdick. The Kinematics of Hyper-Redundant Robot Locomotion. *IEEE Transactions on Robotics and Automation*, 11(6):781–793, 1995.

[31] Hyun-Taek Choi and Junku Yuh. *Underwater Robots*. 2016.

[32] Howie Choset, Kevin M. Lynch, Seth Hutchinson, George a. Kantor, Wolfram Burgard, Lydia E. Kavraki, and Sebastian Thrun. *Principles of Robot Motion*. Number C. 2005.

[33] M. Cianchetti, F. Renda, A. Licofonte, and C. Laschi. Sensorization of continuum soft robots for reconstructing their spatial configuration. *Proceedings of the IEEE RAS and EMBS International Conference on Biomedical Robotics and Biomechatronics*, pages 634–639, 2012.

[34] R. Colbaugh, M. Trabatti, and K. Glass. Redundant nonholonomic mechanical systems: characterization and control. *Robotica*, 17(2):203–217, 1999.

[35] Fionnuala Connolly, Panagiotis Polygerinos, Conor J. Walsh, and Katia Bertoldi. Mechanical Programming of Soft Actuators by Varying Fiber Angle. *Soft Robotics*, 2(1):26–32, 2015.

[36] Fionnuala Connolly, Conor J. Walsh, and Katia Bertoldi. Automatic design of fiber-reinforced soft actuators for trajectory matching. *Proceedings of the National Academy of Sciences*, 114(1):51–56, 2017.

[37] By Cosimo, Della Santina, Matteo Bianchi, Giorgio Grioli, Franco Angelini, Manuel Catalano, Manolo Garabini, and Antonio Bicchi. Controlling Soft Robots. pages 75–83.

[38] Lara S Cowan and Ian D Walker. "Soft" Continuum Robots : the Interaction of Continuous and Discrete Elements. pages 126–133, 2008.

[39] Raphael Deimel and Oliver Brock. A novel type of compliant and underactuated robotic hand for dexterous grasping. *International Journal of Robotics Research*, 35(1-3), 2016.

[40] Michal Karol Dobrzynski, Ramon Pericet-Camara, and Dario Floreano. Contactless deflection sensor for soft robots. *IEEE International Conference on Intelligent Robots and Systems*, pages 1913–1918, 2011.

[41] Dylan Drotman, Saurabh Jadhav, Mahmood Karimi, Philip Dezonia, and Michael T. Tolley. 3D printed soft actuators for a legged robot capable of navigating unstructured terrain. *Proceedings - IEEE International Conference on Robotics and Automation*, pages 5532–5538, 2017.

[42] Christian Duriez and Christian Duriez. Finite Element Method Control of Elastic Soft Robots based on Real-Time Finite Element Method. pages 3967–3972, 2013.

[43] Khaled Elgeneidy, Gerhard Neumann, Michael Jackson, and Niels Lohse. Directly Printable Flexible Strain Sensors for Bending and Contact Feedback of Soft Actuators. *Frontiers in Robotics and AI*, 5(February):1–14, 2018.

[44] Yahya Elsayed, Augusto Vincensi, Constantina Lekakou, Tao Geng, C. M. Saaj, Tommaso Ranzani, Matteo Cianchetti, and Arianna Menciassi. Finite Element

Analysis and Design Optimization of a Pneumatically Actuating Silicone Module for Robotic Surgery Applications. *Soft Robotics*, 1(4):255–262, 2014.

[45] Egidio Falotico, Lorenzo Vannucci, Nicola Di Lecce, Paolo Dario, and Cecilia Laschi. A bio-inspired model of visual pursuit combining feedback and predictive control for a humanoid robot. *Proceedings of the 17th International Conference on Advanced Robotics, ICAR 2015*, (July):188–193, 2015.

[46] Nicholas Farrow, Yang Li, and Nikolaus Correll. Morphological and Embedded Computation in a Self-contained Soft Robotic Hand. 2016.

[47] Wyatt Felt. *Sensing Methods for Soft Robotics*. 2017.

[48] Wyatt Felt, Khai Yi Chin, and C. David Remy. Smart Braid Feedback for the Closed-Loop Control of Soft Robotic Systems. *Soft Robotics*, 00(00):soro.2016.0056, 2017.

[49] Thomas George Thuruthel, Egidio Falotico, Mariangela Manti, Andrea Pratesi, Matteo Cianchetti, and Cecilia Laschi. Learning Closed Loop Kinematic Controllers for Continuum Manipulators in Unstructured Environments. *Soft Robotics*, 00(00):soro.2016.0051, 2017.

[50] Giada Gerboni, Alessandro Diodato, Gastone Ciuti, Matteo Cianchetti, and Arianna Menciassi. Feedback Control of Soft Robot Actuators via Commercial Flex Bend Sensors. *IEEE/ASME Transactions on Mechatronics*, 22(4):1881–1888, 2017.

[51] Giada Gerboni, Alessandro Diodato, Gastone Ciuti, Matteo Cianchetti, and Arianna Menciassi. Feedback Control of Soft Robot Actuators via Commercial Flex Bend Sensors. *IEEE/ASME Transactions on Mechatronics*, 22(4):1881–1888, 2017.

[52] Giada Gerboni, Alessandro Diodato, Gastone Ciuti, Matteo Cianchetti, and Arianna Menciassi. Feedback control of soft robot actuators via commercial flex bend sensors. *IEEE/ASME Transactions on Mechatronics*, 22(4):1881–1888, 2017.

[53] Tim Giffney, Mengying Xie, Aaron Yong, Andrew Wong, Philippe Mousset, Andrew McDaid, and Kean Aw. Soft Pneumatic Bending Actuator with Integrated Carbon Nanotube Displacement Sensor. *Robotics*, 5(1):7, 2016.

[54] Michele Giorelli, Federico Renda, Marcello Calisti, Andrea Arienti, Gabriele Ferri, and Cecilia Laschi. Neural Network and Jacobian Method for Solving the Inverse Statics of a Cable-Driven Soft Arm with Nonconstant Curvature. *IEEE Transactions on Robotics*, 31(4):823–834, 2015.

[55] Paul Glick, Srinivasan Suresh, Donald Ruffatto III, Mark Cutkosky, Michael T. Tolley, and Aaron Parness. A soft robotic gripper with gecko-inspired adhesive. *IEEE Robotics and Automation Letters*, 3766(c):1–1, 2018.

[56] Michael D. Grissom, Vilas Chitrakaran, Dustin Dienno, Matthew Csencits, Michael Pritts, Bryan Jones, William McMahan, Darren Dawson, Chris Rahn, and Ian

Walker. Design and experimental testing of the OctArm soft robot manipulator. 6230:62301F, 2006.

[57] Michael W. Hannan and Ian D. Walker. Kinematics and the Implementation of an Elephant's Trunk Manipulator and Other Continuum Style Robots. *Journal of Robotic Systems*, 20(2):45–63, 2003.

[58] Jonathan Hiller and Hod Lipson. Automatic design and manufacture of soft robots. *IEEE Transactions on Robotics*, 28(2):457–466, 2012.

[59] Shigeo Hirose. *Biologically inspired robots: snake-like locomotors and manipulators*, volume 1093. Oxford university press Oxford, 1993.

[60] Filip Ilievski, Aaron D Mazzeo, Robert F Shepherd, Xin Chen, and George M Whitesides. Soft robotics for chemists. *Angewandte Chemie*, 123(8):1930–1935, 2011.

[61] Filip Ilievski, Aaron D. Mazzeo, Robert F. Shepherd, Xin Chen, and George M. Whitesides. Soft robotics for chemists. *Angewandte Chemie - International Edition*, 50(8):1890–1895, 2011.

[62] Rongjie Kang, Emanuele Guglielmino, David T. Branson, and Darwin G. Caldwell. Bio-inspired crawling locomotion of a multi-arm octopus-like continuum system. *IEEE International Conference on Intelligent Robots and Systems*, pages 145–150, 2012.

[63] Apoorva Kapadia and Ian D. Walker. Task-space control of extensible continuum manipulators. *2011 IEEE/RSJ International Conference on Intelligent Robots and Systems*, pages 1087–1092, 2011.

[64] Apoorva D. Kapadia, Katelyn E. Fry, and Ian D. Walker. Empirical investigation of closed-loop control of extensible continuum manipulators. *IEEE International Conference on Intelligent Robots and Systems*, (Iros):329–335, 2014.

[65] Sangbae Kim, Matthew Spenko, Salomon Trujillo, Barrett Heyneman, Virgilio Mattoli, and Mark R. Cutkosky. Whole body adhesion: Hierarchical, directional and distributed control of adhesive forces for a climbing robot. *Proceedings - IEEE International Conference on Robotics and Automation*, (April):1268–1273, 2007.

[66] Maris Knite, Valdis Teteris, Aleksandra Kiploka, and Jevgenijs Kaupuzs. Polyisoprene-carbon black nanocomposites as tensile strain and pressure sensor materials. *Sensors and Actuators A: Physical*, 110(1-3):142–149, 2004.

[67] Naveen Kuppuswamy and Juan-Pablo Carbajal. Learning a curvature dynamic model of an octopus-inspired soft robot arm using flexure sensors. *Procedia Computer Science*, 7:294–296, 2011.

[68] Frederick Largilliere, Valerian Verona, Eulalie Coevoet, Mario Sanz-Lopez, Jeremie Dequidt, and Christian Duriez. Real-time control of soft-robots using asynchronous

finite element modeling. *2015 IEEE International Conference on Robotics and Automation (ICRA)*, pages 2550–2555, 2015.

[69] Cecilia Laschi and Matteo Cianchetti. Soft Robotics: New Perspectives for Robot Bodyware and Control. *Frontiers in Bioengineering and Biotechnology*, 2(January):1–5, 2014.

[70] Cecilia Laschi, Matteo Cianchetti, Barbara Mazzolai, Laura Margheri, Maurizio Follador, and Paolo Dario. Soft robot arm inspired by the octopus. *Advanced Robotics*, 26(7):709–727, 2012.

[71] Chiwon Lee, Myungjoon Kim, Yoon Jae Kim, Nhayoung Hong, Seungwan Ryu, H. Jin Kim, and Sungwan Kim. Soft robot review. *International Journal of Control, Automation and Systems*, 15(1):3–15, 2017.

[72] Taeyoung Lee, Melvin Leok, and N. Harris McClamroch. Geometric numerical integration for complex dynamics of tethered spacecraft. *Proceedings of the 2011 American Control Conference*, (March):1885–1891, 2011.

[73] Zheng Li, Liao Wu, Hongliang Ren, and Haoyong Yu. Kinematic comparison of surgical tendon-driven manipulators and concentric tube manipulators. *Mechanism and Machine Theory*, 107(June 2016):148–165, 2017.

[74] P. Liljebck, K. Y. Pettersen, O. Stavdahl, and J. T. Gravdahl. A review on modelling, implementation, and control of snake robots. *Robotics and Autonomous Systems*, 60(1):29–40, 2012.

[75] Huai Ti Lin, Gary G. Leisk, and Barry Trimmer. GoQBot: A caterpillar-inspired soft-bodied rolling robot. *Bioinspiration and Biomimetics*, 6(2), 2011.

[76] Ming Luo, Yixiao Pan, Erik H. Skorina, Weijia Tao, Fuchen Chen, Selim Ozel, and Cagdas D. Onal. Slithering towards autonomy: A self-contained soft robotic snake platform with integrated curvature sensing. *Bioinspiration and Biomimetics*, 10(5), 2015.

[77] Ming Luo, Erik H. Skorina, Weijia Tao, Fuchen Chen, Selim Ozel, Yinan Sun, and Cagdas D. Onal. Toward Modular Soft Robotics: Proprioceptive Curvature Sensing and Sliding-Mode Control of Soft Bidirectional Bending Modules. *Soft Robotics*, 4(2):117–125, 2017.

[78] M. Manti, A. Pratesi, E. Falotico, M. Cianchetti, and C. Laschi. Soft assistive robot for personal care of elderly people. *2016 6th IEEE International Conference on Biomedical Robotics and Biomechatronics (BioRob)*, pages 833–838, 2016.

[79] Mariangela Manti, Taimoor Hassan, Giovanni Passetti, Nicolò D'Elia, Cecilia Laschi, and Matteo Cianchetti. A Bioinspired Soft Robotic Gripper for Adaptable and Effective Grasping. *Soft Robotics*, 2(3):107–116, 2015.

[80] Andrew D. Marchese, Robert K. Katzschmann, and Daniela Rus. Whole arm planning for a soft and highly compliant 2D robotic manipulator. *IEEE International Conference on Intelligent Robots and Systems*, pages 554–560, 2014.

[81] Andrew D. Marchese, Konrad Komorowski, Cagdas D. Onal, and Daniela Rus. Design and control of a soft and continuously deformable 2D robotic manipulation system. *Proceedings - IEEE International Conference on Robotics and Automation*, pages 2189–2196, 2014.

[82] Andrew D. Marchese, Cagdas D. Onal, and Daniela Rus. Autonomous Soft Robotic Fish Capable of Escape Maneuvers Using Fluidic Elastomer Actuators. *Soft Robotics*, 1(1):75–87, 2014.

[83] Andrew D. Marchese and D. Rus. Design, kinematics, and control of a soft spatial fluidic elastomer manipulator. *The International Journal of Robotics Research*, pages 0278364915587925–, 2015.

[84] Andrew D. Marchese, Russ Tedrake, and Daniela Rus. Dynamics and trajectory optimization for a soft spatial fluidic elastomer manipulator. *International Journal of Robotics Research*, 35(8):1000–1019, 2016.

[85] Ramses V. Martinez, Jamie L. Branch, Carina R. Fish, Lihua Jin, Robert F. Shepherd, Rui M.D. Nunes, Zhigang Suo, and George M. Whitesides. Robotic

tentacles with three-dimensional mobility based on flexible elastomers. *Advanced Materials*, 25(2):205–212, 2013.

[86] William McMahan, Bryan A. Jones, and Ian D. Walker. Design and implementation of a multi-section continuum robot: Air-octor. *2005 IEEE/RSJ International Conference on Intelligent Robots and Systems, IROS*, pages 3345–3352, 2005.

[87] Bobak Mosadegh, Panagiotis Polygerinos, Christoph Keplinger, Sophia Wennstedt, Robert F. Shepherd, Unmukt Gupta, Jongmin Shim, Katia Bertoldi, Conor J. Walsh, and George M. Whitesides. Pneumatic networks for soft robotics that actuate rapidly. *Advanced Functional Materials*, 24(15), 2014.

[88] Philip Moseley, Juan Manuel Florez, Harshal Arun Sonar, Gunjan Agarwal, William Curtin, and Jamie Paik. Modeling, Design, and Development of Soft Pneumatic Actuators with Finite Element Method. *Advanced Engineering Materials*, 18(6):978–988, 2016.

[89] NDI. Aurora tracking sensors.

[90] Pham Huy Nguyen, Saivimal Sridar, Wenlong Zhang, and Panagiotis Polygerinos. Design and control of a 3-chambered fiber reinforced soft actuator with off-the-shelf stretch sensors. *International Journal of Intelligent Robotics and Applications*, 1(3):342–351, 2017.

[91] Mihoko Otake, Yoshiharu Kagami, Masayuki Inaba, and Hirochika Inoue. Motion design of a starfish-shaped gel robot made of electro-active polymer gel. *Robotics and Autonomous Systems*, 40(2-3):185–191, 2002.

[92] Selim Ozel, Nehir A. Keskin, Darien Khea, and Cagdas D. Onal. A precise embedded curvature sensor module for soft-bodied robots. *Sensors and Actuators, A: Physical*, 236:349–356, 2015.

[93] Snehal Pardeshi. ESP8266 IoT Platform- ESP-12E and NodeMCU, 2017.

[94] Sung-Jin Park, Mattia Gazzola, Kyung Soo Park, Shirley Park, Valentina Di Santo, Erin L Blevins, Johan U Lind, Patrick H Campbell, Stephanie Dauth, Andrew K Capulli, et al. Phototactic guidance of a tissue-engineered soft-robotic ray. *Science*, 353(6295):158–162, 2016.

[95] Yong Lae Park and Robert J. Wood. Smart pneumatic artificial muscle actuator with embedded microfluidic sensing. *Proceedings of IEEE Sensors*, pages 1–4, 2013.

[96] Saint Paul, Ryan S Penning, Jinwoo Jung, Nicola J Ferrier, and Michael R Zinn. An Evaluation of Closed - Loop Control Options for Continuum Manipulators. pages 5392–5397, 2012.

[97] Ryan S Penning, Jinwoo Jung, Justin Borgstadt, Nicola J Ferrier, Michael R Zinn, and Others. Towards closed loop control of a continuum robotic manipulator for

medical applications. *Robotics and Automation (ICRA), 2011 IEEE International Conference on*, pages 4822–4827, 2011.

[98] R Pfeifer, M Lungarella, and F Iida. Self- Organization, Embodiment, and Biologically Inspired Robotics. *Science*, 318(November):1088–1093, 2007.

[99] Rolf Pfeifer. Visual servo control of cable-driven soft robotic manipulator. *2013 IEEE/RSJ International Conference on Intelligent Robots and Systems*, pages 57–62, 2013.

[100] Brennan T Phillips, Kaitlyn P Becker, Shunichi Kurumaya, Kevin C Galloway, Daniel Vogt, Clark Teeple, Michelle H Rosen, David F Gruber, and J Robert. Dexterous Deep-Sea Soft Robotic Arms : A low-power soft manipulator for biological exploration. (Whitcomb 2000).

[101] Panagiotis Polygerinos, Zheng Wang, Kevin C. Galloway, Robert J. Wood, and Conor J. Walsh. Soft robotic glove for combined assistance and at-home rehabilitation. *Robotics and Autonomous Systems*, 73:135–143, nov 2015.

[102] Panagiotis Polygerinos, Zheng Wang, Kevin C. Galloway, Robert J. Wood, and Conor J. Walsh. Soft robotic glove for combined assistance and at-home rehabilitation. In *Robotics and Autonomous Systems*, volume 73, 2015.

[103] F. Renda, M. Cianchetti, M. Giorelli, A. Arienti, and C. Laschi. A 3D steady-state model of a tendon-driven continuum soft manipulator inspired by the octopus arm. *Bioinspiration and Biomimetics*, 7(2), 2012.

[104] Federico Renda, Michele Giorelli, Marcello Calisti, Matteo Cianchetti, and Cecilia Laschi. Dynamic model of a multibending soft robot arm driven by cables. *IEEE Transactions on Robotics*, 30(5), 2014.

[105] Federico Renda, Michele Giorelli, Scuola Superiore, Sant Anna, Scuola Superiore, Sant Anna, Federico Renda, Michele Giorelli, Student Member, Marcello Calisti, and Matteo Cianchetti. Dynamic Model of a Multibending Soft Robot Arm Driven by Cables Dynamic Model of a Multibending Soft Robot Arm Driven by Cables. *IEEE Transactions on Robotics*, 30(October):1–14, 2014.

[106] Federico Renda, Francesco Giorgio-Serchi, Frederic Boyer, Cecilia Laschi, Jorge Dias, and Lakmal Seneviratne. A unified multi-soft-body dynamic model for underwater soft robots. *The International Journal of Robotics Research*, 37(6):648–666, 2018.

[107] Graham Robinson and J Bruce C Davies. Continuum robots-a state of the art. In *Robotics and Automation, 1999. Proceedings. 1999 IEEE International Conference on*, volume 4, pages 2849–2854. IEEE, 1999.

[108] Ellen T. Roche, Markus A. Horvath, Isaac Wamala, Ali Alazmani, Sang Eun Song, William Whyte, Zurab Machaidze, Christopher J. Payne, James C. Weaver, Gregory Fishbein, Joseph Kuebler, Nikolay V. Vasilyev, David J. Mooney, Frank A. Pigula, and Conor J. Walsh. Soft robotic sleeve supports heart function. *Science Translational Medicine*, 9(373):1–12, 2017.

[109] Daniela Rus and Michael T Tolley. Design, fabrication and control of soft robots Terms of Use Design, fabrication and control of soft robots. *Nature*, 521(7553):467–475, 2015.

[110] Cosimo Della Santina, Robert K Katzschmann, Antonio Bicchi, and Daniela Rus. Dynamic Control of Soft Robots Interacting with the Environment. 2018.

[111] Sina Sareh, Yohan Noh, Min Li, Tommaso Ranzani, Hongbin Liu, and Kaspar Althoefer. Macrobend optical sensing for pose measurement in soft robot arms. *Smart Materials and Structures*, 24(12):125024, 2015.

[112] Joshua Schultz, Yiğit Mengüç, Michael Tolley, and Bram Vanderborght. What Is the Path Ahead for Soft Robotics? *Soft Robotics*, 3(4):159–160, 2016.

[113] Yoel Shapiro, Gabor Kosa, and Alon Wolf. Shape tracking of planar hyper-flexible beams via embedded PVDF deflection sensors. *IEEE/ASME Transactions on Mechatronics*, 19(4):1260–1267, 2014.

[114] Robert F Shepherd, Filip Ilievski, Wonjae Choi, Stephen A Morin, Adam A Stokes, Aaron D Mazzeo, Xin Chen, Michael Wang, and George M Whitesides. Multigait soft robot. *Proceedings of the national academy of sciences*, 108(51):20400–20403, 2011.

[115] Nabil Simaan, Russell Taylor, and Paul Flint. A dexterous system for laryngeal surgery. In *Robotics and Automation, 2004. Proceedings. ICRA'04. 2004 IEEE International Conference on*, volume 1, pages 351–357. IEEE, 2004.

[116] Erik H. Skorina, Ming Luo, Weijia Tao, Fuchen Chen, Jie Fu, and Cagdas D. Onal. Adapting to Flexibility: Model Reference Adaptive Control of Soft Bending Actuators. *IEEE Robotics and Automation Letters*, 2(2):964–970, 2017.

[117] Smooth-On. Ecoflex.

[118] Seppe Terryn, Joost Brancart, Dirk Lefeber, Guy Van Assche, and Bram Vanderborght. Self-healing soft pneumatic robots. *Science Robotics*, 2(9):eaan4268, 2017.

[119] Thomas George Thuruthel, Egidio Falotico, Matteo Cianchetti, Federico Renda, and Cecilia Laschi. Learning Global Inverse Statics Solution for a Redundant Soft Robot. *Proceedings of the 13th International Conference on Informatics in Control, Automation and Robotics*, pages 303–310, 2016.

[120] Michael T. Tolley, Robert F. Shepherd, Bobak Mosadegh, Kevin C. Galloway, Michael Wehner, Michael Karpelson, Robert J. Wood, and George M. Whitesides. A Resilient, Untethered Soft Robot. *Soft Robotics*, 1(3):213–223, 2014.

[121] Manas M Tonapi, Isuru S Godage, AM Vijaykumar, and Ian D Walker. A novel continuum robotic cable aimed at applications in space. *Advanced Robotics*, 29(13):861–875, 2015.

[122] Deepak Trivedi, Amir Lotfi, and Christopher D. Rahn. Geometrically exact dynamic models for soft robotic manipulators. *2007 IEEE/RSJ International Conference on Intelligent Robots and Systems*, 24(4):1497–1502, 2007.

[123] Deepak Trivedi, Christopher D Rahn, William M Kier, and Ian D Walker. Soft robotics: Biological inspiration, state of the art, and future research. *Applied bionics and biomechanics*, 5(3):99–117, 2008.

[124] Deepak Trivedi, Christopher D. Rahn, William M. Kier, and Ian D. Walker. Soft robotics: Biological inspiration, state of the art, and future research. *Applied Bionics and Biomechanics*, 5(3):99–117, 2008.

[125] Stephen Tully, Andrea Bajo, George Kantor, Howie Choset, and Nabil Simaan. Constrained filtering with contact detection data for the localization and registration of continuum robots in flexible environments. *Proceedings - IEEE International Conference on Robotics and Automation*, pages 3388–3394, 2012.

[126] Stephen Tully, George Kantor, Marco a Zenati, and Howie Choset. Shape Estimation for Image-Guided Surgery with a Highly Articulated Snake Robot Highly Articulated Snake Robot. pages 1353–1358, 2011.

[127] T. Umedachi, V. Vikas, and B. A. Trimmer. Softworms: The design and control of non-pneumatic, 3D-printed, deformable robots. *Bioinspiration and Biomimetics*, 11(2):0, 2016.

[128] Robert J. Webster and Bryan A. Jones. Design and kinematic modeling of constant curvature continuum robots: A review. *International Journal of Robotics Research*, 29(13):1661–1683, 2010.

[129] Michael Wehner, Ryan L. Truby, Daniel J. Fitzgerald, Bobak Mosadegh, George M. Whitesides, Jennifer A. Lewis, and Robert J. Wood. An integrated design and fabrication strategy for entirely soft, autonomous robots. *Nature*, 536(7617), 2016.

[130] Kai Xu and Nabil Simaan. An investigation of the intrinsic force sensing capabilities of continuum robots. *IEEE Transactions on Robotics*, 24(3):576–587, 2008.

[131] Y. Yekutieli. Dynamic Model of the Octopus Arm. II. Control of Reaching Movements. *Journal of Neurophysiology*, 94(2):1459–1468, 2005.

[132] Michael C. Yip and David B. Camarillo. Model-Less Hybrid Position/Force Control: A Minimalist Approach for Continuum Manipulators in Unknown, Con-

strained Environments. *IEEE Robotics and Automation Letters*, 1(2):844–851, 2016.

[133] Hongying Zhang and Michael Yu Wang. Multi-Axis Soft Sensors Based on Dielectric Elastomer. *Soft Robotics*, 3(1):3–12, 2016.